



Article

# Abnormal Expression of Synaptic and Extrasynaptic GABA<sub>A</sub> Receptor Subunits in the Dystrophin-Deficient *mdx* Mouse

Faouzi Zarrouki <sup>1,2</sup>, Sébastien Goutal <sup>3</sup>, Ophélie Vacca <sup>2</sup> , Luis Garcia <sup>2</sup>, Nicolas Tournier <sup>3</sup> , Aurélie Goyenvalle <sup>2,†</sup> and Cyrille Vaillend <sup>1,\*,†</sup>

<sup>1</sup> Université Paris-Saclay, CNRS, Institut des Neurosciences Paris Saclay, 91400 Saclay, France

<sup>2</sup> Université Paris-Saclay, UVSQ, Inserm, END-ICAP, 78000 Versailles, France

<sup>3</sup> Université Paris-Saclay, INSERM, CNRS, CEA, Laboratoire d'Imagerie Biomédicale Multimodale (BioMaps), Service Hospitalier Frédéric Joliot, 91401 Orsay, France

\* Correspondence: cyrille.vaillend@universite-paris-saclay.fr

† These authors contributed equally to this work.

**Abstract:** Duchenne muscular dystrophy (DMD) is a neurodevelopmental disorder primarily caused by the loss of the full-length Dp427 dystrophin in both muscle and brain. The basis of the central comorbidities in DMD is unclear. Brain dystrophin plays a role in the clustering of central gamma-aminobutyric acid A receptors (GABA<sub>A</sub>Rs), and its loss in the *mdx* mouse alters the clustering of some synaptic subunits in central inhibitory synapses. However, the diversity of GABAergic alterations in this model is still fragmentary. In this study, the analysis of in vivo PET imaging of a benzodiazepine-binding site radioligand revealed that the global density of central GABA<sub>A</sub>Rs is unaffected in *mdx* compared with WT mice. In contrast, semi-quantitative immunoblots and immunofluorescence confocal imaging in tissue sections revealed complex and differential patterns of alterations of the expression levels and/or clustered distribution of a variety of synaptic and extrasynaptic GABA<sub>A</sub>R subunits in the hippocampus, cerebellum, cortex, and spinal cord. Hence, dystrophin loss not only affects the stabilization of synaptic GABA<sub>A</sub>Rs but also influences the subunit composition of GABA<sub>A</sub>Rs subtypes at both synaptic and extrasynaptic sites. This study provides new molecular outcome measures and new routes to evaluate the impact of treatments aimed at compensating alterations of the nervous system in DMD.

**Keywords:** Duchenne muscular dystrophy; GABAergic synapses; PET brain imaging; immunofluorescence; western blots; GABA<sub>A</sub>-receptor clustering; outcome measures



**Citation:** Zarrouki, F.; Goutal, S.; Vacca, O.; Garcia, L.; Tournier, N.; Goyenvalle, A.; Vaillend, C. Abnormal Expression of Synaptic and Extrasynaptic GABA<sub>A</sub> Receptor Subunits in the Dystrophin-Deficient *mdx* Mouse. *Int. J. Mol. Sci.* **2022**, *23*, 12617. <https://doi.org/10.3390/ijms232012617>

Academic Editors: Paola Imbrici and Maria Cristina D'Adamo

Received: 18 July 2022

Accepted: 11 October 2022

Published: 20 October 2022

**Publisher's Note:** MDPI stays neutral with regard to jurisdictional claims in published maps and institutional affiliations.



**Copyright:** © 2022 by the authors. Licensee MDPI, Basel, Switzerland. This article is an open access article distributed under the terms and conditions of the Creative Commons Attribution (CC BY) license (<https://creativecommons.org/licenses/by/4.0/>).

## 1. Introduction

Duchenne muscular dystrophy (DMD) is a lethal X-linked inherited neuromuscular disorder caused by mutations in the gene encoding dystrophin, a cytoskeletal protein normally expressed in both muscles and in the central nervous system (CNS). The DMD syndrome is characterized by progressive muscular degeneration and a neurodevelopmental disorder including a range of central comorbidities, the presence and severity of which depend on the position of the mutations that may alter the expression of several brain dystrophin isoforms encoded by internal promoters [1,2]. The absence of the 427-kDa full-length dystrophin, Dp427, is shared by all patients and is associated with mild cognitive deficits and enhanced emotional reactivity [1,3]. The main mechanistic hypothesis arose from the finding that Dp427 is expressed in principal neurons of brain structures involved in cognitive and behavioral processes, where it colocalizes with a subset of gamma-aminobutyric acid A (GABA<sub>A</sub>) receptors (GABA<sub>A</sub>Rs) [4] and appears to regulate their clustering and/or molecular composition in the postsynaptic densities (PSDs) of central inhibitory synapses [5,6]. These processes are essential for the proper development and function of GABAergic synapses, and their alteration likely plays a role

in the etiology of neurodevelopmental disorders by influencing brain connectivity, activity, and plasticity [7].

GABA<sub>A</sub>Rs are GABA-gated, chloride-selective channels located either at the inhibitory synapse mediating fast, phasic synaptic inhibition, or at extrasynaptic sites mediating tonic inhibition [8]. GABA<sub>A</sub>Rs are heteropentameric assemblies that contain at least three different subunits assembled from more than 20 subunits including  $\alpha$ 1–6,  $\beta$ 1–4,  $\gamma$ 1–4,  $\delta$ ,  $\rho$ 1–3,  $\epsilon$ ,  $\theta$ , and  $\pi$ . The majority contain pairs of a single type of  $\alpha$ - and  $\beta$ -subunit variants, associated with the  $\gamma$ 2-subunit required for the binding site of the positive modulator, benzodiazepine. However, minor populations of non-stoichiometric, hybrid receptors containing two different  $\alpha$  subunits have also been reported [9–11]. Combinations containing  $\alpha$ 1-3,  $\beta$ , and  $\gamma$  subunits are mostly represented at the synaptic site, while those containing  $\alpha$ 4-6,  $\beta$ , and  $\delta$  subunits are mostly extrasynaptic [12,13]. The subunit identity of GABA<sub>A</sub>Rs, which determines their pharmacological and physiological properties, not only depends on their subcellular localization but also varies during development and across brain structures [14,15]. Moreover, various anchoring and trafficking mechanisms regulate the density and size of postsynaptic GABA<sub>A</sub>Rs clusters during synapse formation and maturation, likely in an activity-dependent manner [5,16,17].

Dp427 dystrophin has several molecular partners at the postsynaptic membrane of inhibitory synapses, which together form the dystrophin-associated complex [2] showing interactions with PSD proteins involved in the regulation of GABA<sub>A</sub>Rs clustering, such as the synaptic scaffolding molecule (S-SCAM) and the transsynaptic neuroligin-neurexin complex [18]. However, the impact of Dp427 loss on the density and molecular heterogeneity of GABA<sub>A</sub>Rs is still ill-defined. While Dp427 is dispensable for the initial gephyrin-dependent anchoring of GABA<sub>A</sub>Rs [4], its absence in *mdx* mice, a mouse model of DMD lacking Dp427, is associated with significant decreases in the density and size of clusters containing the  $\alpha$ 1 subunit in the cerebellum and the  $\alpha$ 2 subunit in the hippocampus and amygdala [6,19,20]. A series of studies also demonstrated changes in GABAergic inhibitory transmission and their impact on synaptic plasticity and emotional behaviors in this mouse model [19,21–28]. In all, it is believed that the Dp427-associated complex stabilizes large GABA<sub>A</sub>R clusters at the synapse, perhaps by limiting their lateral diffusion, thereby playing a critical role in the molecular and functional long-term maintenance of inhibitory synapses. Interestingly, an electrophysiological study in cerebellar slices [29] and an in vivo pharmacological experiment [23] both revealed an enhanced sensitivity of *mdx* mice to a selective activator of extrasynaptic GABA<sub>A</sub>Rs, suggesting a change in the density and/or composition of these receptors. However, the molecular studies in *mdx* mice have to date been restricted to the  $\alpha$ 1 and  $\alpha$ 2 subunits. This should be extended to the expression and distribution of several synaptic and extrasynaptic subunits in various brain structures to better understand the impact of Dp427 loss on inhibitory networks and to identify robust and specific molecular outcome measures for preclinical rescue experiments [20,30,31].

In the present study, we first used in vivo positron emission tomography (PET) imaging of brains from WT and Dp427-deficient (*mdx*) mice with the benzodiazepine-binding site radioligand [<sup>11</sup>C]flumazenil, referred to as a translational tool to investigate disease-induced changes in the GABA<sub>A</sub>R density in both clinical [32,33] and preclinical studies [34,35]. In distinct cohorts of mice, we then undertook a detailed evaluation of expression levels and clustering of a variety of GABA<sub>A</sub>R subunits ex vivo, using semi-quantitative Western blotting (WB) and immunofluorescence (IF) techniques, respectively. We selected brain areas with expected relevance to the *mdx* mouse behavioral phenotype and high expression of Dp427 (hippocampus, cerebellum, and cortex). We also analyzed tissue samples from the cervical spinal cord, as the expression of dystrophins in this part of the nervous system has been largely overlooked despite a demonstrated expression of GABA<sub>A</sub>R subunits [15,36,37], and as putative changes in peripheral inhibition might affect mouse behavior. Our PET imaging study shows that the density of main synaptic GABA<sub>A</sub>Rs is unaffected by dystrophin loss, and therefore insufficient to identify relevant translational readouts. In contrast, fine semi-quantitative analyses of tissue samples and

sections reveal a complex pattern of changes in expression and distribution of several synaptic and extrasynaptic GABA<sub>A</sub>R subunits in *mdx* mice.

## 2. Results

### 2.1. In Vivo [<sup>11</sup>C]Flumazenil Brain PET Imaging

In both WT and *mdx* mice, higher uptake of [<sup>11</sup>C]flumazenil was observed in GABA<sub>A</sub>R rich regions such as the hippocampus, and lower uptake was seen in the brain stem and hypothalamus (Figure 1). This is consistent with the reported brain distribution of this radioligand in mice [34]. The brain kinetics of [<sup>11</sup>C]flumazenil were strikingly similar in WT and *mdx* mice, in all tested brain regions (Figure 1A–G). There was no significant difference in the area under the time-activity curve of [<sup>11</sup>C]flumazenil between WT and *mdx* mice, in any brain regions, including the brain stem, which was used as a reference to estimate [<sup>11</sup>C]flumazenil binding to GABA<sub>A</sub>Rs ( $p < 0.05$ ). There was no significant genotype difference in the corresponding [<sup>11</sup>C]flumazenil binding potential (BP<sub>ND</sub>) in any tested brain region (all  $p > 0.05$ ; Figure 1H). Voxel-to-voxel analysis was then performed to investigate sub-regional change in [<sup>11</sup>C]flumazenil BP<sub>ND</sub> and we found no cluster with a significant difference in BP<sub>ND</sub> between parametric images obtained in WT and *mdx* mice. An unconventional normalization of the BP<sub>ND</sub> to the striatum was also attempted, as the striatum can be considered as a pseudo-reference structure devoid of dystrophin [6,38], which led to the same conclusion (Supplementary Figure S1). Altogether, no difference in [<sup>11</sup>C]flumazenil binding could be observed in *mdx* compared with control mice, suggesting the absence of macroscopically detectable change in GABA<sub>A</sub>Rs expression.

### 2.2. Western Blot Analyses

To characterize genotype differences in the expression level of the main subunits composing GABA<sub>A</sub>Rs, we used a panel of antibodies that covers the majority of subunits reported to show large expression in the nervous system ( $\alpha 1$ ,  $\alpha 2$ ,  $\alpha 3$ ,  $\alpha 4$ ,  $\alpha 5$ ,  $\alpha 6$ ,  $\beta 1$ ,  $\beta 2$ ,  $\beta 3$ ,  $\gamma 2$ , and  $\delta$ ). We performed a series of semi-quantitative Western blot analyses using protein extracts from the hippocampus, cortex, cerebellum, and spinal cord of the same individuals. To improve the reliability of our comparative quantifications, all samples from a given structure from both genotypes ( $n = 7$ – $8$  mice per genotype) were deposited on the same gel and expression levels were then normalized to vinculin. Figures 2–5 show the expression levels of GABA<sub>A</sub>R subunits in *mdx* mice expressed as percent of WT mean levels.

Hippocampal samples (Figure 2A,B) from *mdx* mice showed a 40% decrease in the expression level of the  $\alpha 2$  subunit ( $p < 0.0205$ ), a 35% decrease for the  $\beta 2$  subunit ( $p < 0.0082$ ), and a 42.5% decrease for the  $\beta 3$  subunit ( $p = 0.0041$ ) as compared with WT, while all other subunits had an expression level comparable to that of WT mice.

Cortex samples (Figure 3A,B) showed a 48.5% increase in the expression level of the  $\alpha 1$  subunit ( $p = 0.0037$ ) and, in the opposite, a 35% decrease in the expression level of the  $\alpha 2$  subunit ( $p = 0.0175$ ) in *mdx* mice. A trend for a decreased expression was observed for the  $\beta 1$  ( $p = 0.07$ ) and  $\delta$  ( $p = 0.05$ ) subunits, and for an increased expression for the  $\gamma 2$  subunit ( $p = 0.07$ ), but these genotype differences did not reach significance. In the cerebellum (Figure 4A,B), there was no significant genotype difference in the expression levels of all subunits.

GABA<sub>A</sub>Rs are also detected in the spinal cord [15,36,37] and prior preliminary results suggested that the Dp427 dystrophin could be expressed at low levels in this tissue (not shown). Using the sensitive Jess Western blot system, we demonstrated that Dp427 is expressed in the cervical spinal cord of WT mice, but not in *mdx* mice, and we further determined that its level of expression is 3–4 times lower in this tissue as compared to the cortex (Supplementary Figure S2). Interestingly, we also found significant variations in the expression level of several GABA<sub>A</sub>R subunits in the cervical spinal cord of *mdx* mice (Figure 5A,B), characterized by increases in expression levels for the  $\alpha 3$  (40%;  $p = 0.0289$ ) and  $\alpha 6$  (25%;  $p = 0.0289$ ) subunits, and conversely, a 56% decrease for the  $\alpha 4$  subunit ( $p = 0.0175$ ).

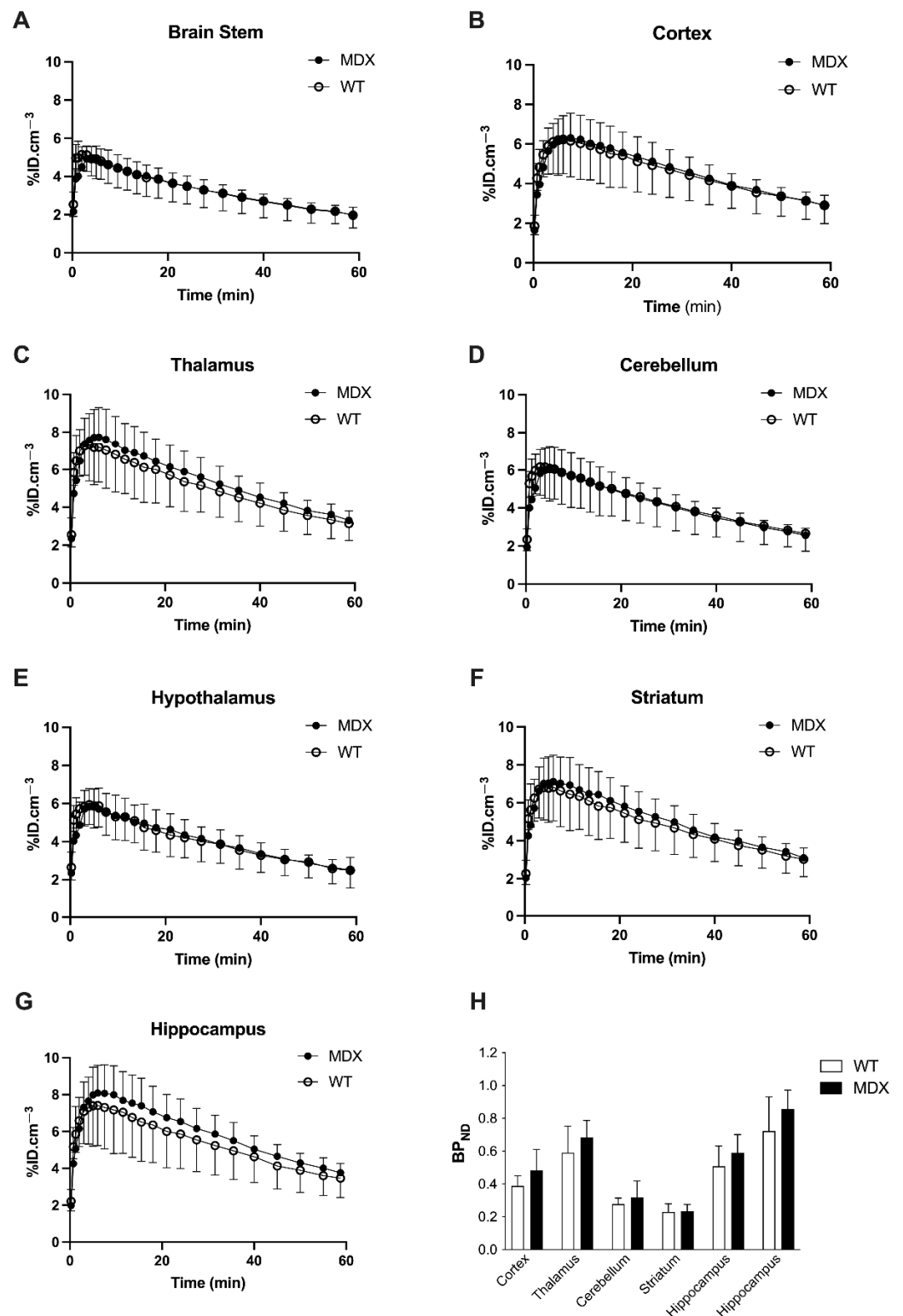


**Figure 1.** In vivo [<sup>11</sup>C]flumazenil positron emission tomography (PET) brain imaging. (A–G) Time-activity curves of [<sup>11</sup>C]flumazenil in the brain stem, cortex, thalamus, cerebellum, hypothalamus, striatum, and hippocampus of wild-type (WT, white symbols and bars,  $n = 5$ ) and *mdx* mice (black symbols and bars,  $n = 6$ ). (H) Corresponding binding potential (BP<sub>ND</sub>) to gamma-aminobutyric acid A receptors (GABA<sub>A</sub>Rs), estimated using the brain stem as a reference region. Data are shown as mean  $\pm$  S.D. Difference in BP<sub>ND</sub> between WT and *mdx* mice was not significant (All  $p > 0.05$ ).

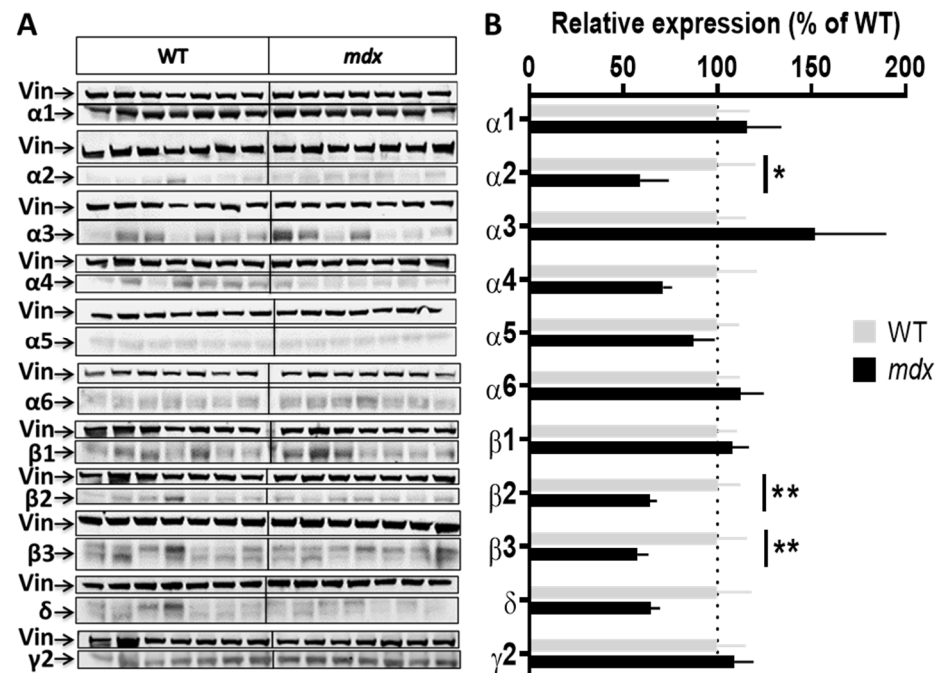


**Figure 2.** Expression level of GABA<sub>A</sub>R subunits in the hippocampus. (A) Immunoblots showing the detection of 11 GABA<sub>A</sub>R subunits in hippocampal extracts from 7 WT and 7 *mdx* mice loaded on the same gels. As indicated, vinculin was used as a loading control for each blot. (B) Quantification of each GABA<sub>A</sub>R subunit normalized to WT level (gray bars, dotted line) to reflect their relative expression (% of WT) in *mdx* mice (black bars). Data are shown as mean ± S.E.M.; significant differences between genotypes are shown by asterisks (\*  $p < 0.05$ , \*\*  $p < 0.01$ ).

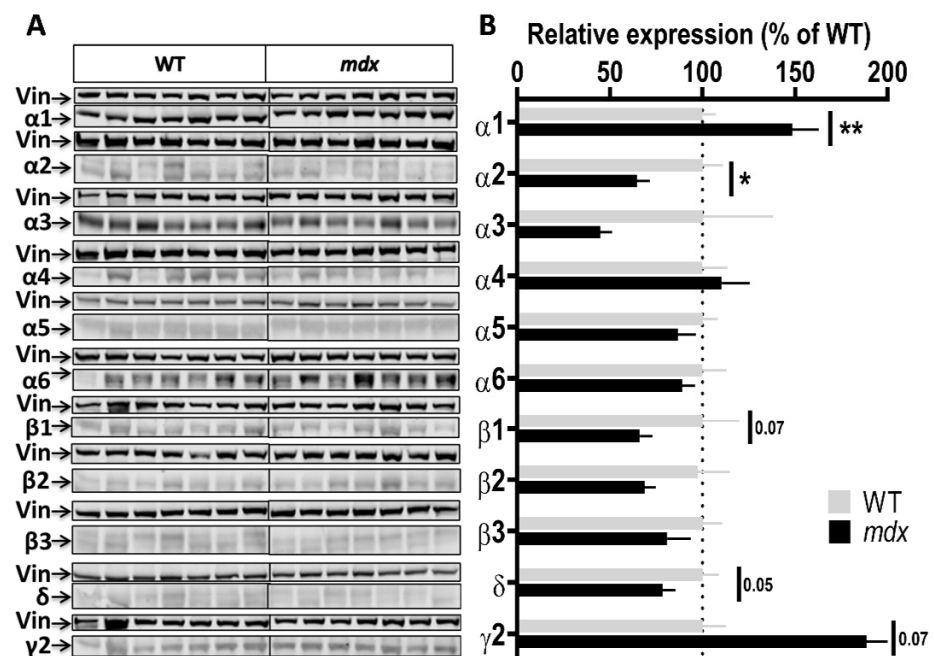


**Figure 3.** Expression level of GABA<sub>A</sub>R subunits in the cortex. (A) Immunoblots showing the detection of 11 GABA<sub>A</sub>R subunits in cortex extracts from 7 WT and 7 *mdx* mice loaded on the same gels. As indicated, vinculin was used as a loading control for each blot. (B) Quantification of each GABA<sub>A</sub>R subunit normalized to WT level (gray bars, dotted line) to reflect their relative expression (% of WT) in *mdx* mice (black bars). Data are shown as mean ± S.E.M.; significant differences between genotypes are shown by asterisks (\*  $p < 0.05$ , \*\*  $p < 0.01$ ). Marginal differences are also indicated ( $p = 0.05$  or  $0.07$ ).

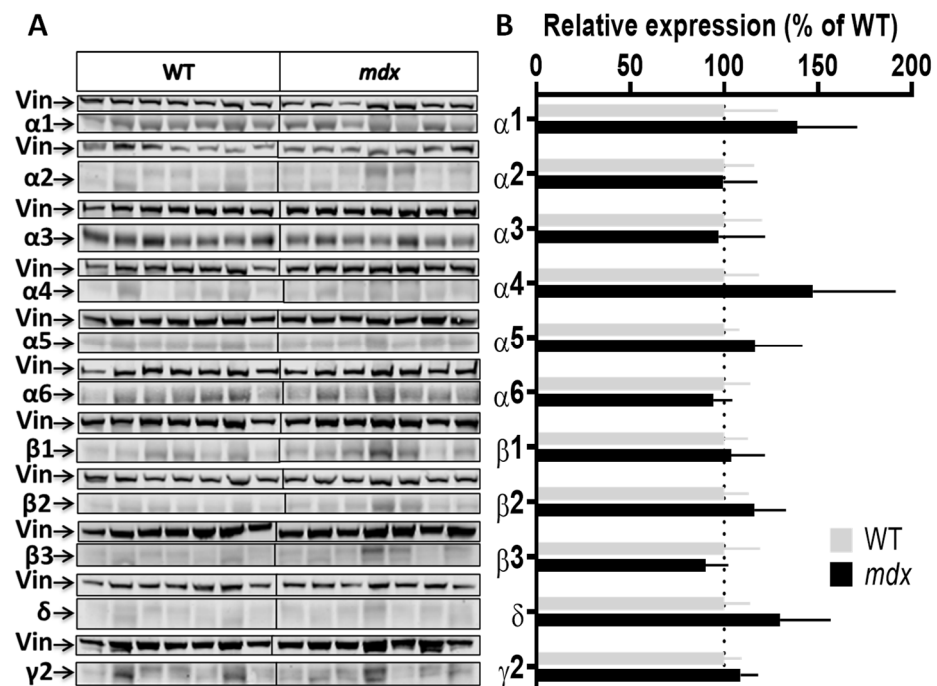


**Figure 4.** Expression level of GABA<sub>A</sub>R subunits in the cerebellum. (A) Immunoblots showing the detection of 11 GABA<sub>A</sub>R subunits in cerebellar extracts from 7 WT and 7 *mdx* mice loaded on the same gels. As indicated, vinculin was used as a loading control for each blot. (B) Quantification of each GABA<sub>A</sub>R subunit normalized to WT level (gray bars, dotted line) to reflect their relative expression (% of WT) in *mdx* mice (black bars). Data are shown as mean ± S.E.M.; no significant difference was found between genotypes in this structure.

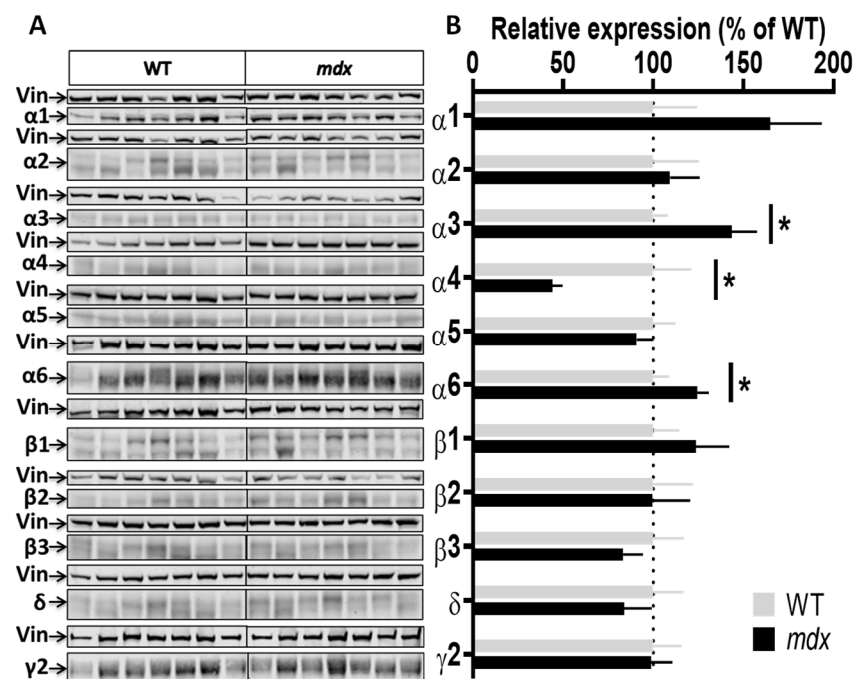


**Figure 5.** Expression level of GABA<sub>A</sub>R subunits in the cervical spinal cord. (A) Immunoblots showing the detection of 11 GABA<sub>A</sub>R subunits in cervical spinal cord extracts from 7 WT and 7 *mdx* mice loaded on the same gels. As indicated, vinculin was used as a loading control for each blot. (B) Quantification of each GABA<sub>A</sub>R subunit normalized to WT level (gray bars, dotted line) to reflect their relative expression (% of WT) in *mdx* mice (black bars). Data are shown as mean ± S.E.M.; significant differences between genotypes are shown by asterisks (\* *p* < 0.05).

A synthesis of the genotype differences revealed by our Western blot study is shown in Table 1, highlighting the selective structure-dependent alterations in expression levels of GABA<sub>A</sub>R subunits in *mdx* mice.

**Table 1.** Summary of Western blot data. Main increases (upward arrows) and decreases (downward arrows) in the expression level of the different GABA<sub>A</sub>R subunits in *mdx* mice are shown for hippocampus (HIP), cerebellum (CBL), cortex (CX), and spinal cord (SC). Probabilities are shown for non-significant (marginal) differences and significant genotype differences are indicated by asterisks (\*  $p < 0.05$ , \*\*  $p < 0.01$ ).

	Western Blot Quantification			
	HIP	CBL	CX	SC
$\alpha 1$	-	-	** ↑	-
$\alpha 2$	* ↓	-	* ↓	-
$\alpha 3$	-	-	-	* ↑
$\alpha 4$	-	-	-	* ↓
$\alpha 5$	-	-	-	-
$\alpha 6$	-	-	-	* ↑
$\beta 1$	-	-	0.07 ↓	-
$\beta 2$	** ↓	-	-	-
$\beta 3$	** ↓	-	-	-
$\gamma 2$	-	-	0.07 ↑	-
$\delta$	-	-	0.05 ↓	-

### 2.3. Immunofluorescence Analyses

A complementary IF study was then undertaken in brain tissue sections ( $n = 5$  mice per genotype) to test specific questions that were raised by the Western blot analyses but could not be addressed by this technique.

First, we wondered whether the opposing changes in the expression levels of  $\alpha 1$  and  $\alpha 2$  subunits in the cortex of *mdx* mice in the WB study could reflect changes in the proportion of receptors containing both the  $\alpha 1$  and  $\alpha 2$  subunits, a hypothesis previously suggested by others [18]. To address this question, we analyzed the 3D colocalization of these two subunits in confocal stack images from sensory-motor cortex sections. As shown in Figure 6, more than 20% of  $\alpha 1$  and  $\alpha 2$  clusters were colocalized in both genotypes, thus suggesting that heteropentamers containing both subunits were indeed present in this region. Interestingly, the percentage of colocalization of  $\alpha 1$  and  $\alpha 2$  subunits was significantly larger in *mdx* mice (43.57%) than in WT mice (29.42%) ( $p = 0.0317$ ), suggesting a marked change in the subunit composition of GABA<sub>A</sub>Rs in cortical synapses of *mdx* mice.

Our Western blot analyses also suggested that subunits known to be predominantly extrasynaptic ( $\alpha 4$ ,  $\alpha 5$ ,  $\alpha 6$ , and  $\delta$ ) were expressed at comparable levels in brain structures of the two genotypes, while  $\alpha 4$  and  $\alpha 6$  subunit expression was significantly and selectively altered in the spinal cord. This was inconsistent with a previous report showing that cerebellar Purkinje neurons of *mdx* mice have an enhanced sensitivity to a selective pharmacological activator of extrasynaptic GABA<sub>A</sub>Rs [29]. We therefore hypothesized that fine alterations in the distribution of these receptors in brain structures could not be detected by a global protein quantification from tissue extracts. To test this hypothesis, we investigated the number, size, and distribution of clusters of  $\alpha 4$ ,  $\alpha 5$ , and  $\alpha 6$  subunits in sections of different brain structures using IF.

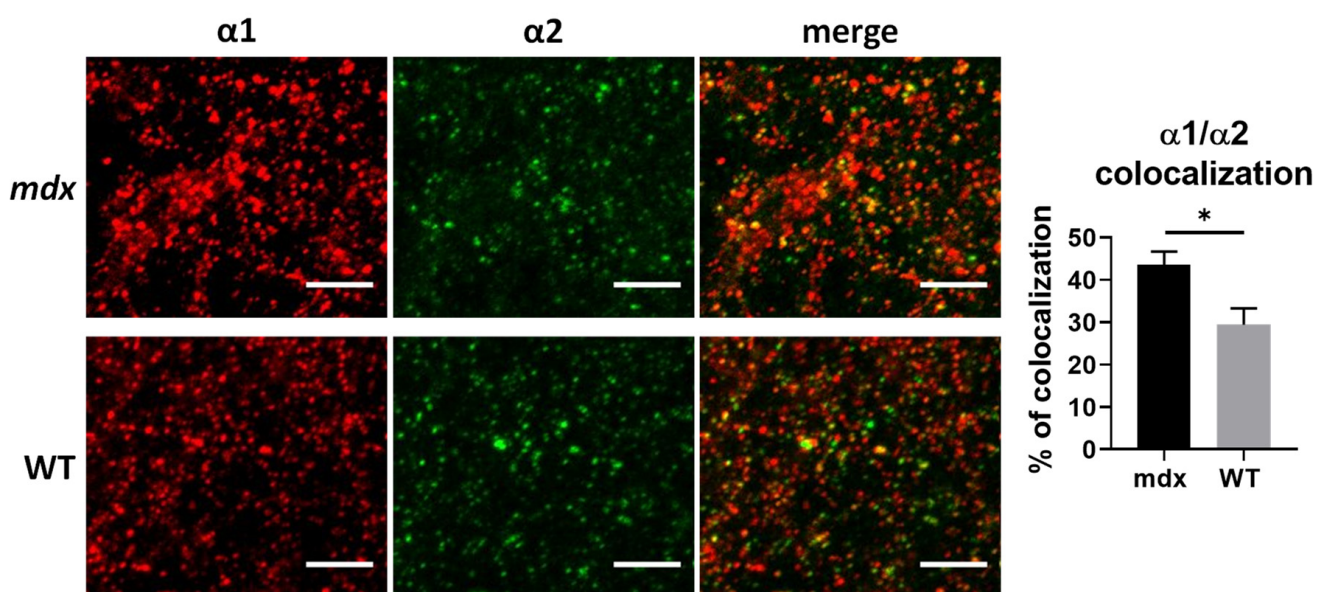


**Figure 6.** Colocalization of  $\alpha1$  and  $\alpha2$  GABA<sub>A</sub>R subunits in the cortex. The left panel shows representative sample confocal laser scanning microscope images of  $\alpha1$ -subunit (red) and  $\alpha2$ -subunit (green) immunoreactive signals, as well as merged images of overlaps (yellow dots) between  $\alpha1$ -subunit and  $\alpha2$ -subunit immunoreactivity in WT and *mdx* mice. The histogram on the right shows the fraction (%) of clusters showing overlaps and reflecting presumed colocalization of these two synaptic subunits. Scale bar: 5  $\mu$ m. \*  $p < 0.05$ .

In all structures, the  $\alpha4$ ,  $\alpha5$ , and  $\alpha6$  subunits showed a punctiform immunoreactivity, typical of GABA<sub>A</sub>R cluster labeling. In both the *stratum pyramidale* (SP) and *stratum radiatum* (SR) of the hippocampus (Figure 7A,B, respectively), there were no main genotype differences in the mean number and size of  $\alpha4$ ,  $\alpha5$ , and  $\alpha6$  clusters (All  $p > 0.05$ ). However, in both subregions of the hippocampus, the distribution of the size of  $\alpha4$ -containing clusters showed a significant rightward shift in *mdx* mice compared with WT (SP:  $p < 0.0001$ ; SR:  $p < 0.001$ ), indicating a larger proportion of big clusters containing the  $\alpha4$  subunit in *mdx* mice. This was not observed for  $\alpha5$  and  $\alpha6$ -containing clusters.

In the cerebellar molecular cell layer (MCL) (Figure 8), the mean number and mean size of clusters containing  $\alpha4$ ,  $\alpha5$ , and  $\alpha6$  subunits were comparable in the two genotypes ( $p > 0.05$ ). However, the distribution of cluster sizes in *mdx* mice showed a significant rightward shift for clusters containing the  $\alpha4$  subunit ( $p < 0.0001$ ), and a leftward shift for those containing the  $\alpha6$  subunit ( $p < 0.0001$ ). This suggests a larger proportion of big  $\alpha4$  subunit-containing clusters and of small  $\alpha6$ -containing clusters.

In the sensory-motor cortex (Figure 9), the mean number and size of clusters was comparable between genotypes ( $p > 0.05$ ), but there was a significant leftward shift of the distribution of the sizes of clusters containing the  $\alpha5$  ( $p < 0.0001$ ) and  $\alpha6$  ( $p < 0.005$ ) subunits in *mdx* mice. This suggests that in this cortex, there was a larger proportion of small clusters containing the  $\alpha5$  and  $\alpha6$  subunits in *mdx* mice.

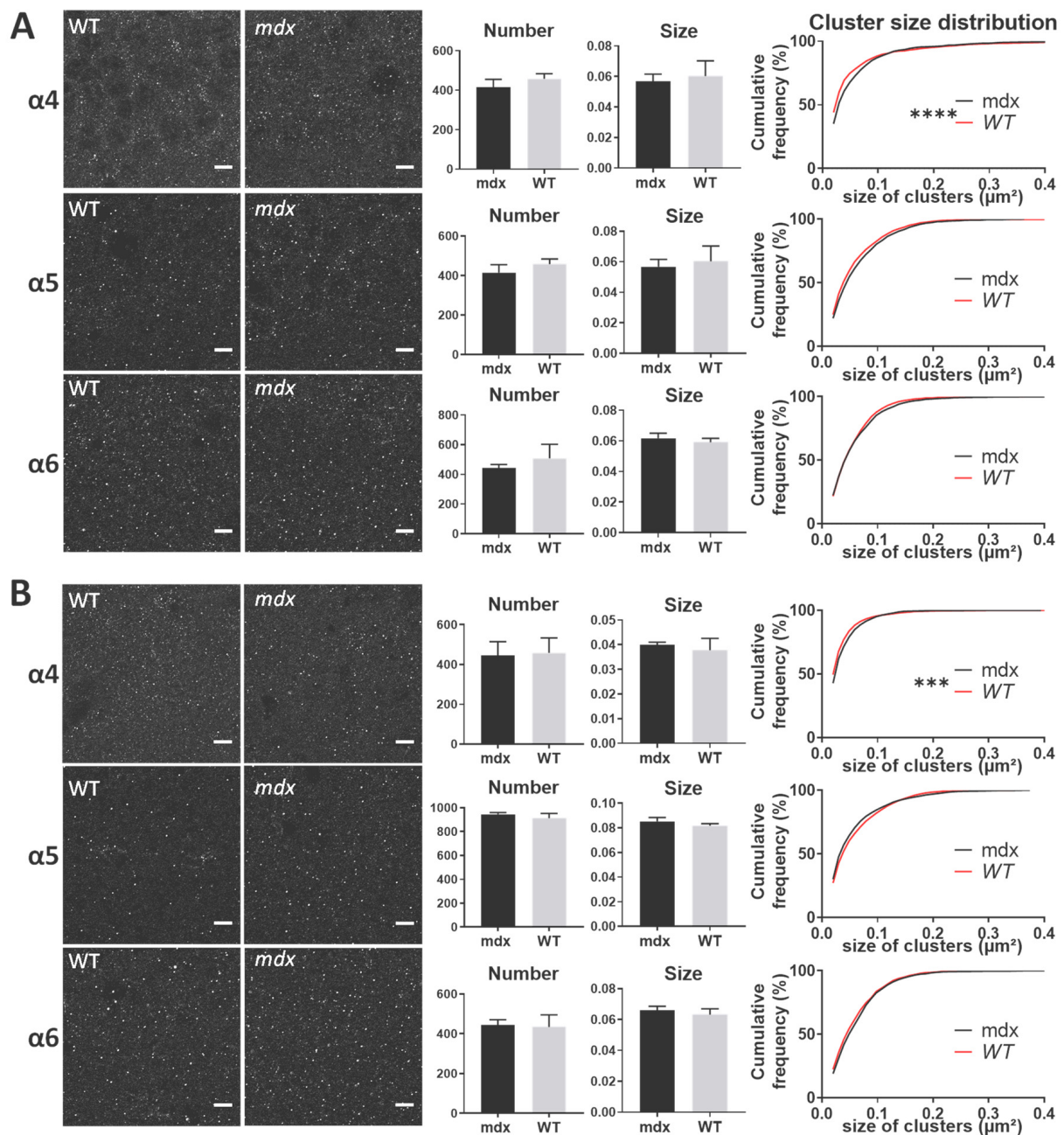


**Figure 7.** Immunohistological analysis of the  $\alpha 4$ – $6$  subunits contained in extrasynaptic GABA<sub>A</sub>Rs in the hippocampus. (A) Analysis in the SP. (B) Analysis in the SR. For each subunit and for both genotypes, from left to right: Representative sample confocal laser scanning microscope images, mean number of clusters, mean cluster size, and distribution curve of the cluster sizes expressed as cumulative frequency (%). Scale bar: 7  $\mu\text{m}$ . \*\*\*\*  $p < 0.0001$ , \*\*\*  $p < 0.001$ .

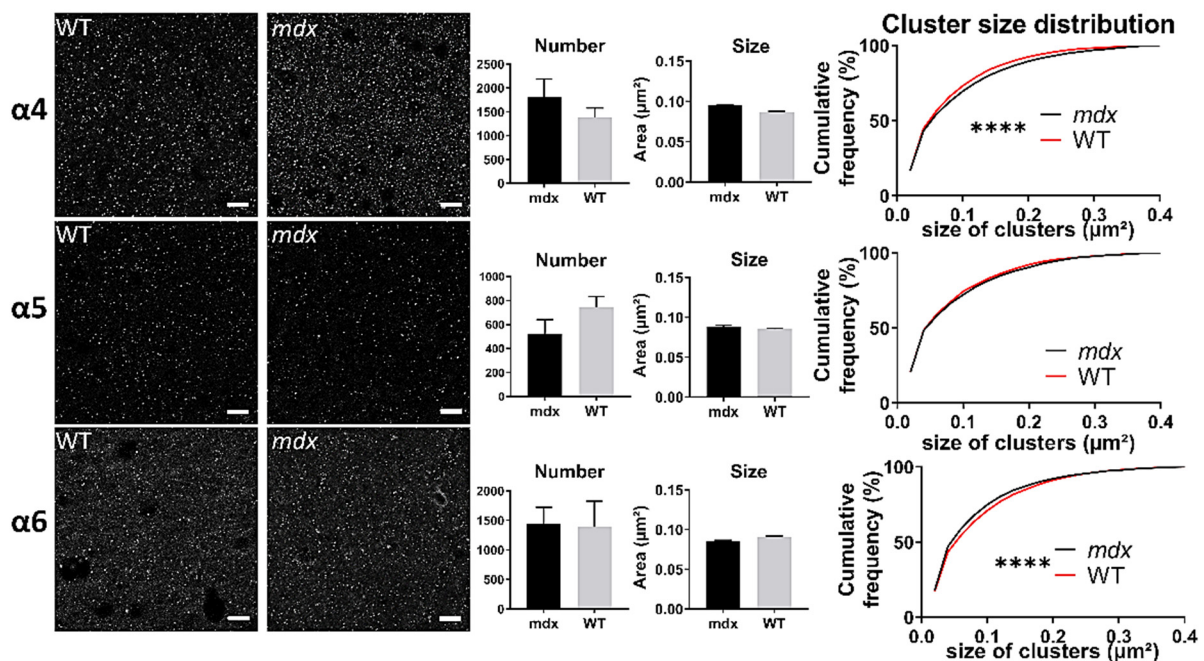


**Figure 8.** Immunohistological analysis of the  $\alpha 4$ – $6$  subunits contained in extrasynaptic GABA<sub>A</sub>Rs in the cerebellum. Analysis in the MCL of cerebellum. For each subunit and for both genotypes, from left to right: Representative sample confocal laser scanning microscope images, mean number of clusters, mean cluster size, and distribution curve of the cluster sizes expressed as cumulative frequency (%). Scale bar: 10  $\mu\text{m}$ . \*\*\*\*  $p < 0.0001$ .

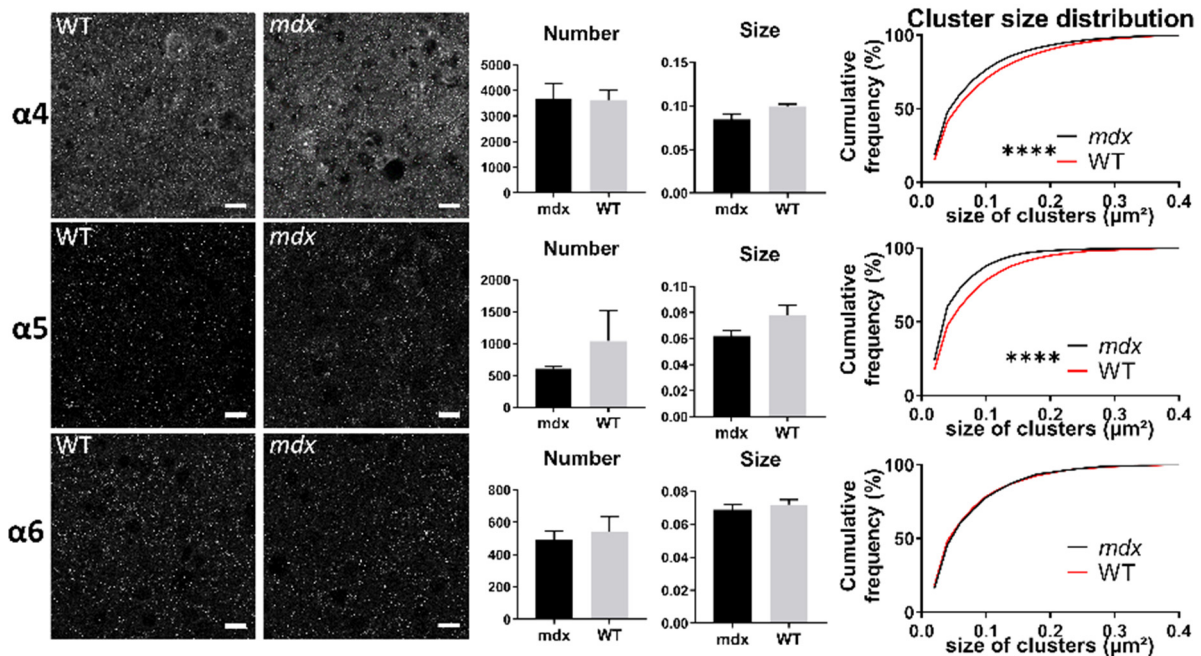


**Figure 9.** Immunohistological analysis of the  $\alpha 4$ – $6$  subunits contained in extrasynaptic GABA<sub>A</sub>Rs in the cortex. Analysis in the sensory-motor cortex. For each subunit and for both genotypes, from left to right: Representative sample confocal laser scanning microscope images, mean number of clusters, mean cluster size, and distribution curve of the cluster sizes expressed as cumulative frequency (%). Scale bar: 10  $\mu\text{m}$ . \*\*\*\*  $p < 0.0001$ .

Table 2 summarizes the significant changes observed in the distribution of the size of clusters containing distinct GABA<sub>A</sub>R subunits.

**Table 2.** Summary of immunohistochemical detection of subunits contained in presumed extrasynaptic GABA<sub>A</sub>Rs. No genotype differences were found for the mean number (Number) and mean size (Size) of clusters containing  $\alpha 4$ ,  $\alpha 5$ , and  $\alpha 6$  subunits. Main shifts in the distribution curves of the cluster sizes are shown. Upward arrows indicate a rightward shift reflecting a larger proportion of big clusters; downward arrows indicate a leftward shift reflecting a larger proportion of small clusters. \*\*\*\*  $p < 0.0001$ , \*\*\*  $p = 0.0007$ .

HIP (SP)	Number	Size	Distribution	HIP (SR)	Number	Size	Distribution
$\alpha 4$	-	-	**** ↑	$\alpha 4$	-	-	*** ↑
$\alpha 5$	-	-	-	$\alpha 5$	-	-	-
$\alpha 6$	-	-	-	$\alpha 6$	-	-	-
CBL	Number	Size	Distribution	CX	Number	Size	Distribution
$\alpha 4$	-	-	**** ↑	$\alpha 4$	-	-	**** ↓
$\alpha 5$	-	-	-	$\alpha 5$	-	-	**** ↓
$\alpha 6$	-	-	**** ↓	$\alpha 6$	-	-	-

### 3. Discussion

Many lines of evidence indicate that the absence of brain full-length dystrophin (Dp427) in DMD mouse models modifies the molecular machinery involved in the formation and long-term maintenance of central inhibitory connectivity. Dp427 loss particularly affects the number, size, and distribution of GABA<sub>A</sub>R clusters containing the  $\alpha 1$  and/or  $\alpha 2$  subunits within certain brain structures [5,39]. Preclinical studies have shown that Dp427 rescue by exon-skipping strategies in the adult brain of *mdx* mice has the potential to restore GABA<sub>A</sub>R clustering, as well as the associated excitatory-synapse plasticity and emotional disturbances [19,20,22,30,31]. This suggests that alterations of local inhibitory networks at least partly underlie the behavioral and cognitive deficits associated with DMD, and that changes in specific GABA<sub>A</sub>R subunits may serve as key readouts to evaluate the efficacy of genetic therapies. However, two studies demonstrated that extrasynaptic GABA<sub>A</sub>Rs may also be affected in *mdx* mice [23,29], implying a more complex pattern of alterations of multiple GABA<sub>A</sub>R subunits. In this study, we therefore used both in vivo and ex vivo approaches to further characterize the number of GABA<sub>A</sub>Rs and the expression of a variety of their subunits in several regions of the nervous system in *mdx* mice. One main objective was to characterize novel molecular outcome measures that could be used in preclinical studies to evaluate the efficacy of therapies targeting the CNS. Brain PET imaging using [<sup>11</sup>C]flumazenil showed that the density of GABA<sub>A</sub>Rs is unaffected by the absence of Dp427 in *mdx* mice, while the expression levels and/or distribution of both synaptic and extrasynaptic GABA<sub>A</sub>R subunits is differentially regulated in distinct brain structures and spinal cord.

#### 3.1. Density of GABA<sub>A</sub>Rs

Our PET imaging study with [<sup>11</sup>C]flumazenil did not reveal any difference between *mdx* and WT mice regarding the total number of GABA<sub>A</sub>Rs in main brain structures that normally express Dp427, such as the hippocampus, cortex, and cerebellum. This seems in contrast with the results obtained in a single photon emitting computed tomography (SPECT) imaging study in DMD patients with a molecule with similar receptor profile, [<sup>123</sup>I]iomazenil, which found a reduction in the density of GABA<sub>A</sub>Rs in the prefrontal cortex of these patients [40]. A difference between the human and mouse conditions cannot be ruled out. However, the lack of genotype identification in the human study did not allow for confirmation that the observed change was specifically due to the lack of Dp427, rather than being influenced by a cumulative deficiency of several dystrophins inducing additional reorganizations of synaptic networks [41,42]. Moreover, the focused analysis of the prefrontal cortex in the patient study does not provide information as to whether

this could be generalized to other brain structures investigated in mice, and an apparent influence of aging on the measurements in patients suggests that additional adaptive factors were involved. Moreover, PET offers absolute quantification whereas SPECT only allows for semi-quantitative interpretation of brain images which may interfere with the interpretation of imaging data [43].

Our present results in *mdx* mice fully agree with previous studies showing that Dp427 loss does not affect the expression of the main GABA<sub>A</sub>Rs anchoring protein, gephyrin, which already suggested that the global density of GABA<sub>A</sub>Rs should not be affected in *mdx* mice. Even though extrasynaptic receptors may be clustered by additional mechanisms involving radixin [44], it was shown that [<sup>11</sup>C]-Flumazenil imaging reflects the density of all types of GABA<sub>A</sub>Rs, including both postsynaptic and extrasynaptic receptors [45,46]. This is a strong argument to conclude that Dp427 loss does not impact the total number of central GABA<sub>A</sub>Rs in mice. Our immunoblot study confirms and elaborates upon this finding, as all of the structures analyzed here show comparable expression of the  $\gamma$ 2 subunit, a specific core component of synaptic GABA<sub>A</sub>Rs, and of the  $\delta$  subunit that characterizes a majority of extrasynaptic receptors. We cannot exclude the possibility that a decrease in the number of receptors per synapse could be masked by a compensatory increase in synapse density, as we have previously shown that there are more inhibitory synapses in the dorsal CA1 hippocampal area of *mdx* mice [43]. In any case, the *in vivo* quantification of GABA<sub>A</sub>R density does not provide a translational tool to evaluate central GABAergic alterations in preclinical studies, because this parameter is not affected by Dp427 loss in *mdx* mice.

As shown in Figure 10 (upper left panel), brain dystrophin in the PSDs of inhibitory synapses is associated with the dystroglycan complex, composed of extracellular  $\alpha$ -dystroglycan ( $\alpha$ -DG) that binds Neuroligin-2, and  $\beta$ -dystroglycan ( $\beta$ -DG) that binds the scaffolding protein S-SCAM and gephyrin-associated IQsec3 (or SynArfGEF) proteins. Dystrophin and dystroglycan appear to be dispensable for the gephyrin-dependent anchoring of GABA<sub>A</sub>Rs [4,6,47], which may explain why the total number of GABA<sub>A</sub>Rs is unaffected in *mdx* mice. However, Dp427 deficiency induces alterations of neuroligin-2 expression and might affect S-SCAM and IQsec3 as well, which may significantly modify the formation, maturation, and long-term maintenance of at least a subset of GABAergic synapses [5,39,48,49]. The reported decrease in the number of clusters containing the synaptic  $\alpha$ 1 and  $\alpha$ 2 subunits in *mdx* mice, as well as their higher sensitivity to selective activators of extrasynaptic receptors, could thus reflect complex changes in the proportion of specific GABA<sub>A</sub>R subtypes or modifications of the subunit assembly [18].

### 3.2. Expression of Synaptic GABA<sub>A</sub>Rs

Our precise semi-quantitative analysis of immunoblots demonstrated that the expression levels of synaptic subunits are differentially regulated in *mdx* mice, and also revealed that selective changes occur depending on the brain structure (Figure 10). Large variation in expression of the different GABA<sub>A</sub>R subunits may exist in the distinct CNS structures, which were analyzed in separate immunoblots to focus on the genotype differences. Putative changes in the relative expression of subunits between structures could not be estimated from these analyses and the genotype differences are therefore discussed for each structure separately.

In the hippocampus, we confirm a significant decrease of the  $\alpha$ 2 subunit expression, which was previously reported in two studies using quantitation of  $\alpha$ 2-containing cluster immunoreactivity in hippocampal sections [6,20]. This also partially correlates with another seminal study [50], which analyzed the expression of  $\alpha$ 1 and  $\alpha$ 2 subunits mRNAs in different brain structures of the *mdx* mouse and reported their decreased expression in the hippocampus. In the present study, we confirm a decrease in  $\alpha$ 2 expression in the hippocampus at the protein level, but we did not detect significant changes in the  $\alpha$ 1 subunit expression. Aside from putative methodological differences between the two studies, protein expression does not always strictly follow changes in transcript expression levels, due to multiple post-transcriptional regulations and putative systemic adaptations and

remodeling of the GABAergic synaptic networks. We also report significant decreases in the expression of the  $\beta 2$  and  $\beta 3$  subunits. Because these two subunits can be associated with the  $\alpha 2$  subunit, one may hypothesize a decrease in the number of synaptic receptors composed of  $\alpha 2\beta 2\gamma 2$  and/or  $\alpha 2\beta 3\gamma 2$  subunits, perhaps partly compensated by  $\alpha 3$ -containing receptors, as we observed a non-significant but noticeable increase (~50%) in the expression level of this subunit.

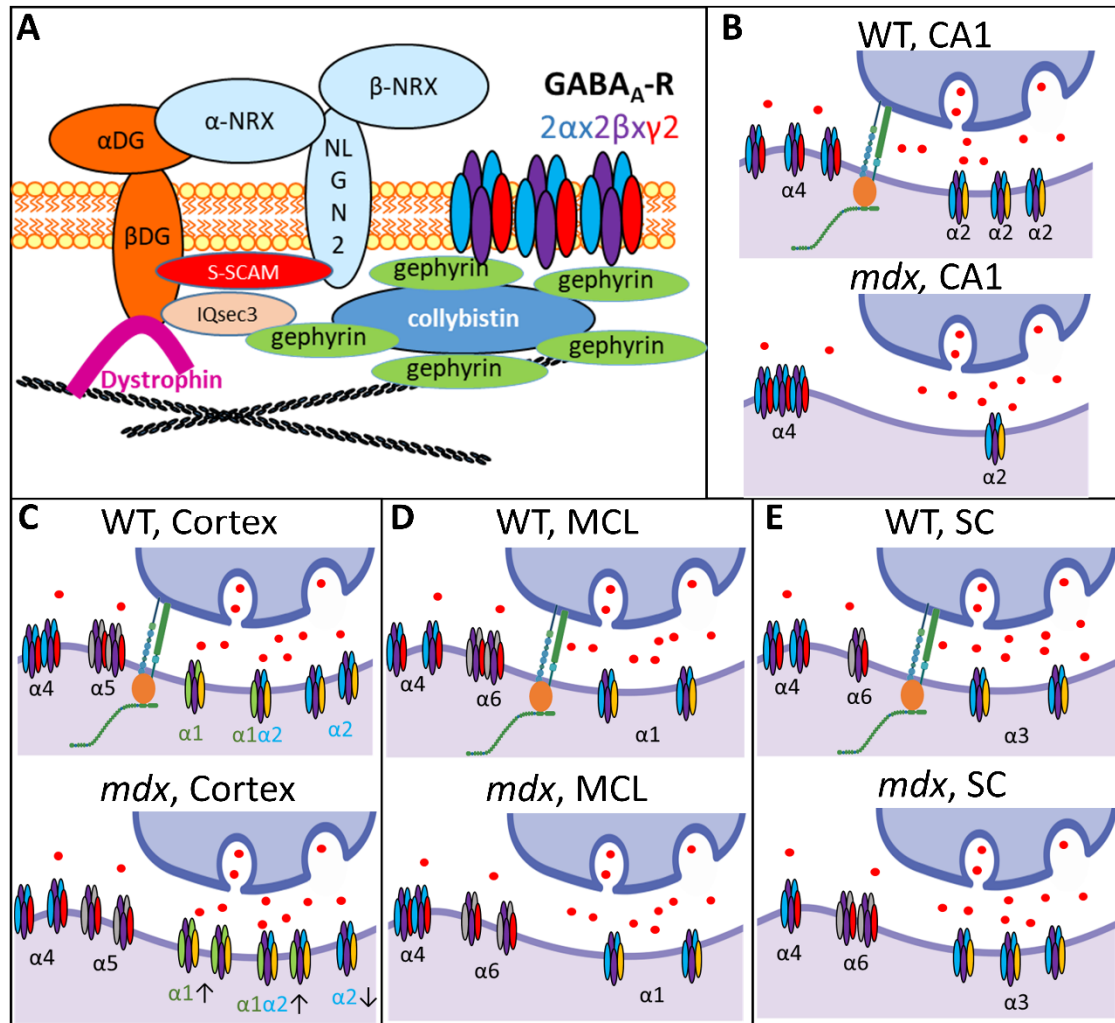


**Figure 10.** Brain dystrophin deficiency and the multiple alterations of GABA<sub>A</sub>-R subtypes in distinct regions of the nervous system. **(A)** Diagram showing the interaction of the dystrophin-associated complex ( $\alpha$  and  $\beta$  dystroglycans) with key postsynaptic scaffolding proteins (Neurologin-2, neurexin, S-SCAM, IQsec3) involved in the regulation of GABA<sub>A</sub>-R clustering in central inhibitory synapses. As indicated in top right corner, the different colors in GABA<sub>A</sub>-Rs correspond to the  $\alpha$  subunits (light blue),  $\beta$  subunits (purple) and  $\gamma 2$  subunits (red). **(B–E)** Schematic summary of the results obtained in this study comparing the expression and distribution of synaptic and extrasynaptic GABA<sub>A</sub>-R subunits in WT and dystrophin-deficient *mdx* mice. The working models combine expression-level data from semi-quantitative immunoblots and distribution of cluster sizes from IF confocal analyses. The main type of  $\alpha$  subunit contained in the displayed receptors is indicated (subunits' colors are arbitrary, but the font color matches the color of the subunits in the drawing when their expression is changed in *mdx* mice). Arrows below isolated synaptic GABA<sub>A</sub>-Rs in the *mdx*-cortex drawing indicate decreased (down) or increased (up) expression levels of specific  $\alpha$  subunits. Adjacent receptors symbolize large clusters. CA1: Hippocampal CA1 area; MCL: molecular cell layer of cerebellum; SC: spinal cord.

In the cerebellum, we found no difference in the expression of all subunits as a function of genotype. This is in line with previous studies showing that changes in  $\alpha 1$  subunit expression in the cerebellum cannot be detected in immunoblots [24], confirming that the total number of receptors containing this subunit is not affected, while their ability to form large clusters is selectively impaired [6].

In the cortex, there was an overexpression of the  $\alpha 1$  subunit and a downregulation of the  $\alpha 2$  subunit, suggesting major changes in the main  $\alpha 1\beta\gamma$  and  $\alpha 2\beta\gamma$  synaptic GABA<sub>A</sub>Rs expressed at the inhibitory synapse. The opposing changes in expression of these two subunits suggested putative changes in the proportion of synapses expressing these receptor subtypes, or subtle modifications in the relative expression of these two GABA<sub>A</sub>R subtypes within the synapse. It is suspected that  $\alpha 1$ - and  $\alpha 2$ -GABA<sub>A</sub>Rs have distinct roles in the formation of GABAergic circuits in close interaction with the dystrophin-glycoprotein complex, but it was also shown that the absence of the  $\alpha 1$  subunit in the hippocampus may induce a compensatory increase in  $\alpha 2$ -containing synapses and a reorganization of inhibitory circuits [16,48]. To further detail this observation, we performed a double immunohistochemical labeling of  $\alpha 1$  and  $\alpha 2$  and analyzed the putative colocalizations of clusters containing these subunits in the cortex. Interestingly, the two subunits colocalized in ~30% of GABA<sub>A</sub>R clusters in WT mice, and there was a significant increase by 10% of this colocalization in *mdx* mice. This suggests that the absence of dystrophin from inhibitory synapses is associated with an increased density of clusters that contain both  $\alpha 1\beta\gamma$  and  $\alpha 2\beta\gamma$  subtypes of GABA<sub>A</sub>Rs. Alternatively, these results may also fit with a working model in which changes in the expression of these subunits in *mdx* mice reflect the presence of hybrid receptors containing both  $\alpha 1$  and  $\alpha 2$ , as suggested by others [18]. Several hybrid GABA<sub>A</sub>Rs containing heterologous  $\alpha 1/\alpha 2$ ,  $\alpha 1/\alpha 3$ , and  $\alpha 2/\alpha 3$  pairs of subunits have been characterized in the mammalian cortex and shown to include the synaptic  $\gamma 2$  subunit and a benzodiazepine-binding site [9–11]. It has been suggested that dystrophin may play a role in the stabilization of GABA<sub>A</sub>R clusters, perhaps by limiting their lateral diffusion along the postsynaptic membrane. To date, however, there is no known mechanism that directly involves dystrophin in the assembly of GABA<sub>A</sub>R subunits, and the present results might reflect an adaptation of inhibitory networks during synaptogenesis [16,48].

### 3.3. Expression of Extrasynaptic GABA<sub>A</sub>Rs

In our immunoblots analysis, the cervical spinal cord was the only structure showing significant changes in the expression level of extrasynaptic GABA<sub>A</sub>R subunits between genotypes. This was characterized by a decreased expression of  $\alpha 4$  and an increased expression of  $\alpha 6$ , in addition to an increased expression of the synaptic  $\alpha 3$  subunit. A non-specific effect of inflammation on peripheral inhibitory synapses cannot be ruled out. Indeed, in *mdx* mice muscle degeneration and regeneration has a retrograde inflammatory effect on the peripheral nervous system, including neurodegenerative processes that specifically reduce the synaptic activity of spinal alpha motoneurons [51]. This represents an overlooked feature of DMD pathophysiology, in which commutative mechanisms in the central and peripheral nervous systems may contribute to motor behavior deficits. However, we demonstrated here that Dp427 is expressed in the spinal cord, yet at a level 3–4 times lower than in brain structures. This suggests that these changes observed in *mdx* mice instead reflect a role played by dystrophin in the clustering of GABA<sub>A</sub>Rs in peripheral inhibitory synapses. Furthermore, the altered expression of extrasynaptic GABA<sub>A</sub>Rs in spinal cord might explain the enhanced behavioral sensitivity of *mdx* mice to gaboxadol, a pharmacological agent that binds preferentially to extrasynaptic subunits  $\alpha 4$ ,  $\alpha 6$ , and  $\delta$  [52]. We previously showed that *mdx* mice more rapidly display a loss of the righting reflex induced by gaboxadol, as do mice overexpressing  $\alpha 6$  subunit-containing extrasynaptic receptors [23,53]. Because gaboxadol was administered intra-peritoneally in this previous study, a contribution of peripheral GABA<sub>A</sub>Rs was therefore possible. Importantly, we show that the  $\alpha 6$  subunit expression is also increased in the spinal cord of *mdx* mice, which further suggests implication of peripheral  $\alpha 6$ -containing GABA<sub>A</sub>Rs in this phenotype [54].

Changes in extrasynaptic GABA<sub>A</sub>Rs in *mdx* mice cannot be limited to the spinal cord, as their higher sensitivity to gaboxadol was also demonstrated *ex vivo* by electrophysiological techniques in Purkinje neurons of acute cerebellar slices [29]. We therefore hypothesized that this phenotype is not associated with bulk changes in the expression level of extrasynaptic GABA<sub>A</sub>Rs, but rather with more discrete modifications of the size and/or distribution of specific extrasynaptic clusters. Using IF and confocal imaging of brain tissue sections, we detected significant changes between genotypes regarding the size of clusters containing the  $\alpha$ 4–6 extrasynaptic subunits in the hippocampus, cortex and cerebellum (Figure 10).

In the CA1 region of the hippocampus, the proportion of big clusters containing  $\alpha$ 4 was larger in *mdx* than in WT mice in both the neuronal and dendritic layers (SP and SR). In the sensory-motor cortex, however, *mdx* mice expressed a larger proportion of small clusters containing the  $\alpha$ 4 and  $\alpha$ 5 subunits. In the cerebellum, *mdx* mice were characterized by big  $\alpha$ 4 clusters and small  $\alpha$ 6 clusters. Interestingly, this shows that changes in the formation of extrasynaptic clusters are not restricted to the cerebellum in *mdx* mice, but may be differentially altered depending on the brain structure. Clustering alterations are not necessarily characterized by a reduced capacity to form large clusters, as larger clusters containing specific subunits were also detected in *mdx* mice, i.e.,  $\alpha$ 4 in the hippocampus and cerebellum. This suggests that distinct structures underwent different reorganization of extrasynaptic GABA<sub>A</sub>Rs within local inhibitory circuits due to the absence of dystrophin. We may assume that such changes occur in extrasynaptic domains because these subunits normally concentrate extrasynaptically. However, future studies could consider other hypotheses, such as the possibility that the absence of Dp427 could favor specific mechanisms allowing extrasynaptic receptors to switch to synaptic domains. In addition to endocytic recycling and lateral diffusion, it has been proposed that a reservoir of extrasynaptic receptors might indeed play a role in the plasticity of inhibitory synapses by supplying the synaptic pool of GABA<sub>A</sub>Rs [55]. In any case, the changes observed here in *mdx* mice likely alter the physiological properties of extrasynaptic GABA<sub>A</sub>Rs and their sensitivity to specific pharmacological compounds such as gaboxadol [8,52]. This may also contribute to a variety of emotional, cognitive, and neuropsychiatric disorders [55–61] including those reported in *mdx* mice and associated with DMD, such as stress reactivity, anxiety, fear memory, and intellectual disability [23].

### 3.4. Concluding Remarks

We demonstrate that the absence of Dp427 brain dystrophin alters the expression level, distribution and subunit composition of multiple synaptic and extrasynaptic GABA<sub>A</sub>Rs in both central and peripheral inhibitory synapses. This strongly suggests that the role of dystrophin in GABAergic synapses is not limited to the stabilization and confinement of GABA<sub>A</sub>Rs in specific synaptic domains, but may also influence the combination of specific receptor subunits that determine their function and pharmacology.

The observed alterations in central synapses differ among brain structures, suggesting the establishment of variable adaptive processes during synaptogenesis and/or adult brain plasticity. Moreover, we cannot exclude that dystrophin may normally interact with only a subset of these subunits, and that part of the observed changes in *mdx* mice reflect compensatory adaptations within GABAergic network rather than a direct effect of dystrophin loss. Our results do not allow to discriminate cytosolic versus membrane-bound receptor subunits. Future studies comparing the total, membrane, and endocytic fractions might help to further determine whether dystrophin-dependent regulations take place at the plasma membrane or during earlier steps of subunits assembly. Nevertheless, the changes we report for extrasynaptic receptors, in line with previous studies showing a higher sensitivity to gaboxadol in *mdx* mice support the need to investigate putative alterations of the lateral diffusion of GABA<sub>A</sub>Rs. Analyses of their expression in membrane fractions would provide limited information regarding the lateral-diffusion hypothesis that should be addressed using specific technologies [62–65].

Our present study combining Western blotting and IF analyses of cluster distribution provides novel insights into the regulations of the GABAergic system in the dystrophin-deficient mouse, which encompass changes of both postsynaptic and extrasynaptic receptors. This should be further detailed in future studies, as it may open the way for innovative pharmacological interventions based on allosteric modulation of specific GABA<sub>A</sub>R subtypes. Importantly, we show that a relevant part of the molecular alterations reported here can be quantified using standard Western blots. This provides new outcome measurement tools that could be easily replicated in laboratories involved in preclinical mouse studies to evaluate the impact of molecular and pharmacological treatments on the central comorbidities associated with the DMD syndrome.

#### 4. Materials and Methods

##### 4.1. Animals

C57BL/10ScSn-*Dmd*<sup>mdx</sup>/J (*mdx*) dystrophin-deficient and C57BL/10ScSnJ littermate (WT) male mice were obtained by mating heterozygous *mdx* females with WT males. Siblings were kept in the same cage (two to five per cage) under a 12-h light-dark cycle (light on: 7:00 a.m.) with food and water ad libitum. Mouse genotype was verified by polymerase chain reaction. Both in vivo and ex vivo experiments were performed in adult male mice aged 3–5 months.

##### 4.2. [<sup>11</sup>C]-Flumazenil PET Imaging: Acquisition Protocol and Imaging Data Analysis

PET imaging experiments were performed on an Inveon microPET scanner (spatial resolution ~1.6 mm; Siemens Healthcare, Knoxville, TN, USA) in anesthetized mice (1.5–2.5% inhaled isoflurane, weight 34.2 ± 3.7 g). [<sup>11</sup>C]flumazenil was formulated in 0.9% aqueous saline with 3% ethanol (*v/v*). The radiochemical purity of [<sup>11</sup>C]flumazenil was >98% and the molar activity at the time of injection was 6.8 ± 0.9 GBq.μmol<sup>-1</sup>. Data acquisition started immediately after intravenous bolus injection of [<sup>11</sup>C]flumazenil (6.8 ± 0.9 MBq) for 60 min.

Dynamic PET images were reconstructed using standard OSEM-2D reconstruction algorithm while correcting for radioactive decay, scatter, and attenuation. PET data analysis was performed using the PMOD software (version 3.8, PMOD Technologies Ltd., Zurich, Switzerland). Brain PET images were co-registered with an MRI template of the mouse brain to define selected regions of interest, consistent with the spatial resolution of the scanner [66]. Regional time-activity curves (TACs) were generated and expressed as percent of injected dose per volume (ID%/cm<sup>3</sup>). Specific binding of [<sup>11</sup>C]flumazenil to GABA<sub>A</sub>Rs in tested brain regions was estimated using the Logan-reference kinetic model. The regional binding-potential (BP<sub>ND</sub>) was estimated using the brain stem, a region with low expression of GABA<sub>A</sub>Rs, as a previously described reference region [34]. Parametric images describing [<sup>11</sup>C]flumazenil BP<sub>ND</sub> were then generated for each animal. The parametric images obtained in each group (*n* = 5 WT and 6 *mdx* mice) were then compared using a statistical parametric mapping (SPM) and a voxel-to-voxel analysis (SPM8 software, London, UK). A brain mask was created from a [<sup>11</sup>C]flumazenil brain mouse template and applied to parametric maps to include cerebral voxels only. Statistical comparisons were then performed using an unpaired *t*-test design to detect significant difference in BP<sub>ND</sub> between groups. A significance level threshold of 0.05 (uncorrected for multiple comparisons) and a minimum cluster size of 200 voxels were selected. Only the clusters that were significant at *p* < 0.05 levels (corrected for multiple comparisons) were considered.

##### 4.3. Western Blot Analyses of GABA<sub>A</sub>R Subunits

Total protein extracts from *mdx* (*n* = 7–8) and WT littermate mice (*n* = 7) were obtained from dissected brain structures (cortex, hippocampus, cerebellum, and cervical spinal cord) treated with RIPA lysis and extraction buffer (ThermoFisher Scientific, Villebon Sur Yvette, France), complemented with SDS powder (5% final) (Bio-Rad, Marnes La Coquette, France). The total protein concentration was determined with the BCA Protein Assay Kit (ThermoFisher Scientific, Villebon Sur Yvette, France). Samples were denatured at

100 °C for 3 min and 25 µg of protein were loaded onto NuPAGE 4–12% Bolt Bis-Tris Plus Protein gels following manufacturer instructions (Invitrogen, Villebon Sur Yvette, France). Membranes were incubated with antibodies directed against various GABA<sub>A</sub>R subunits (Synaptic system, Gottingen, Germany; Merck, Molsheim, France) along with vinculin (Sigma Aldrich, St Quentin Fallavier, France) for normalization (Table 3). All samples of a given structure from both genotypes were deposited on the same gel in order to obtain a reliable quantification. Antibody signals were visualized using the Odyssey CLx system (Li-Cor, Homburg, Germany) and quantification was done using the Empiria Studio software (Li-Cor, Homburg, Germany). The specificity of the primary antibody was checked by omitting the primary antibody, which did not reveal unspecific bands at the expected molecular weight of the target proteins, and/or by using incubation with a control peptide to confirm the specific bands to be quantified (for the antibodies directed against the α1, α3, and α5 subunits). As described by the manufacturer (Synaptic system, Gottingen, Germany), the α2, β1, and β3 antibodies reveal several relatively close bands which are specific of the analyzed subunits, as previously validated using specific KO mice (α2) and/or control peptides (β1 and β3). Both bands were therefore quantified in this study. Data are presented as mean ± SEM. Statistical analyses were performed using the Mann–Whitney U test in the GraphPad 8 software (Prism, San Diego, CA, USA).

**Table 3.** List of antibodies used in Western blots (WB) and immunohistochemistry (IHC).

Primary Antibodies					
Target	Species	Dilution WB	Dilution IHC	Company, Cat.No	
Vinculin	Mouse	1/50	-	Sigma Aldrich, V9131	
α1 subunit	Guinea pig	1/500	1/500	Synaptic System, 224 204	
α2 subunit	Rabbit	1/1000	1/1000	Synaptic System, 224 102	
α3 subunit	Rabbit	1/500	-	Synaptic System, 224 303	
α4 subunit	Rabbit	1/100	1/100	Synaptic System, 224 402	
α5 subunit	Rabbit	1/500	1/500	Synaptic System, 224 502	
α6 subunit	Rabbit	1/500	1/500	Synaptic System, 224 603	
β1 subunit	Guinea pig	1/500	-	Synaptic System, 224 705	
β2 subunit	Guinea pig	1/500	-	Synaptic System, 224 805	
β3 subunit	Mouse	1/500	-	Synaptic System, 224 411	
γ2 subunit	Rabbit	1/1000	-	Synaptic System, 224 003	
δ subunit	Mouse	1/1000	-	Merck, 05-474	
Secondary Antibodies					
Target	Species	Use	Dilution	Fluorophore	Company, Cat.No
Mouse	Goat	WB	1/2000	IRDye 800CW	Li-Cor Biosciences, 926-32210
Rabbit	Goat	WB	1/2000	IRDye 800CW	Li-Cor Biosciences, 926-32211
Guinea Pig	Donkey	WB	1/2000	IRDye 800CW	Li-Cor Biosciences, 926-32411
Rabbit	Goat	IHC	1/400	Alexa 488	Invitrogen, A-11070
Guinea Pig	Goat	IHC	1/400	Alexa 555	Invitrogen, A-21435

#### 4.4. Semi-Quantitative Immunohistochemistry

Fresh-frozen brain cryosections of 30 µm thickness from 5 mice per genotype were collected onto Superfrost®Plus slides (Carl Roth, Karlsruhe, Germany), thawed for 2 min

at room temperature (RT), fixed in acetone/methanol (1:1) for 5 min at  $-20^{\circ}\text{C}$ , washed in PBS, incubated first in a blocking solution for 45 min (10% normal goat serum, 0.3% Triton X-100, and 1% BSA), then overnight at  $4^{\circ}\text{C}$  with the primary antibody (Dilutions: see Table 3), washed and incubated with the secondary antibody (Dilutions: see Table 3). Controls prepared by omitting the primary antibody showed no specific staining. In each genotype, five cryosections were used to analyze each GABA<sub>A</sub>R subunit (one section from  $n = 5$  mice per genotype). All sections paired between *mdx* and WT mice were taken at equivalent stereotaxic coordinates, between Bregma  $-1.22$  to  $-2.46$  mm for coronal sections including hippocampus and cortex, and from lateral 0.12 to 1.20 mm for sagittal sections of the cerebellum [67]. Within each structure, images were taken at equivalent locations and exposure times using a laser scanning confocal microscope (Zeiss LSM 700, x63 objective; Zeiss, Rueil Malmaison, France). Typically, stacks of 8–9 images ( $1024 \times 1024$  pixels) spaced by  $1\ \mu\text{m}$  were recorded at a magnification of 99 nm/pixel. For quantification of GABA<sub>A</sub>R clusters, digital images were processed with the WCIF ImageJ imaging system (Rasband, W.S., ImageJ, U. S. National Institutes of Health, Bethesda, MD, USA) as follows [6,68,69]: The punctate IR for GABA<sub>A</sub>Rs representing presumptive postsynaptic clusters was analyzed semi-quantitatively in the SP and SR layers (10–100  $\mu\text{m}$  below the SP) of the CA1 subfield of dorsal hippocampus, in layers II–VI of the sensory-motor cortex (same sections as for hippocampus) and in the MCL of the cerebellum (lobules 4–6, 10–150  $\mu\text{m}$  from Purkinje-cell layer), which are known to be strongly immunopositive for dystrophin [6,38]. Quantification of GABA<sub>A</sub>R clusters was performed from a single confocal image taken in the middle of the stack. The minimal cluster size was arbitrarily set to  $0.02\ \mu\text{m}^2$ , corresponding to two adjacent pixels at the magnification used. A threshold segmentation algorithm was used for automatic detection of clusters. The mean number and size of the clusters, as well as the distribution of cluster sizes, were analyzed within a total tissue surface of  $10,000\ \mu\text{m}^2$  per animal in each brain structure or subregion. Clusters double-labeled for the  $\alpha 1$  and  $\alpha 2$  GABA<sub>A</sub>R subunits were identified using all images of the stacks with the 3D colocalization analysis tool of the Imaris image analysis software (version 9, Bitplane, Zurich, Switzerland). Data presented as means  $\pm$  SEM were statistically analyzed using the Mann–Whitney U test, while the distributions of the cluster sizes were compared using the Kolmogorov–Smirnov test with a significance threshold set at  $p < 0.005$  (GraphPad 8 software, Prism software, San Diego, CA, USA).

#### 4.5. Detection of Dystrophin in Spinal Cord Using the Automated Jess Western Blot System

Detection of dystrophin expression in the spinal cord was performed using the capillary Western immunoassay Jess system based on the protocol previously described by Beekman et al. [70] and according to the manufacturer's instructions (Bio-Techne, Minneapolis, MN, USA), using a  $66 \pm 440$  kDa Separation Module (ProteinSimple SM-W008), the Anti-Rabbit Detection Module (ProteinSimple DM-001), and the Anti-Mouse Detection Module (ProteinSimple DM-002). Protein samples (1  $\mu\text{g}$ ) were prepared in sample buffer from the Separation Module, then mixed with Fluorescent Master Mix and heated at  $95^{\circ}\text{C}$  for 5 min. The samples, blocking reagent (antibody diluent), primary antibodies (in antibody diluent), HRP-conjugated secondary antibodies, and chemiluminescent substrate were pipetted into the plate (part of Separation Module). Dystrophin expression was detected with a combination of primary antibodies including the mouse monoclonal antibodies, NCL-DYS1 (1/25, Leica Biosystems, Nanterre, France), MANDYS1(3B7) (1/25, Developmental Studies Hybridoma Bank—DSHB, Iowa City, IA, USA) and MANEX58D(7G2) (1/25, Developmental Studies Hybridoma Bank—DSHB), and the rabbit monoclonal ab154168 (1/1000, Abcam, Paris, France). Vinculin was detected with the mouse monoclonal anti-vinculin hVin-1 antibody (1/100, Sigma) as normalization control. Instrument default settings were as follows: stacking and separation at 475 V for 30 min; blocking reagent for 5 min, primary and secondary antibodies for 30 min each; luminol/peroxide chemiluminescence detection for  $\sim 15$  min. The resulting electropherograms were inspected to check whether automatic peak detection required any manual correction. A 6-point calibration curve was loaded,

made of a mix of WT and dystrophin-deficient control lysates to obtain defined percentages of dystrophin (0, 5, 10, 15% or 0, 10, 15, 30% of corresponding WT tissues) as previously described for our Western blot analyses [30].

**Supplementary Materials:** The supporting information can be downloaded at: <https://www.mdpi.com/article/10.3390/ijms232012617/s1>.

**Author Contributions:** C.V., F.Z., A.G., N.T. and L.G. contributed to the conception and design of the study; F.Z., S.G. and O.V. performed experiments; C.V., F.Z., S.G., A.G. and N.T. contributed to the analysis and interpretation of data; F.Z., C.V., S.G., N.T., O.V. and A.G. contributed to drafting the text and figures. All authors have read and agreed to the published version of the manuscript.

**Funding:** This work was supported by Centre National de la Recherche Scientifique (CNRS, France), the Institut National de la santé et la recherche médicale (INSERM), Université Paris-Saclay (France), Paris Ile-de-France Region, a grant to C.V. from Association Monégasque contre les Myopathies (AMM, Monaco), and PhD fellowships from Ministère de l'Enseignement Supérieur et de la Recherche (France) and AFM (Association Française contre les Myopathies, France) to F.Z. We also gratefully acknowledge support to C.V. and A.G. from the European Union's Horizon 2020 research and innovation program "Brain Involvement in Dystrophinopathies" under grant agreement No. 847826.

**Institutional Review Board Statement:** All experimental procedures were conducted under appropriate biological containment in accordance with European Communities Council Directive (CEE 86/609) for animal care and experimentation, EU Directive 2010/63/EU, and French National Committee (87/848), and were approved by ethic committee (Paris Centre et Sud, CEEA59 and A18-065) and the French government.

**Informed Consent Statement:** Not applicable.

**Data Availability Statement:** The data used to support our findings are included within the article and as supplementary data.

**Acknowledgments:** The authors are grateful to the Zootechnic platform of our institutes for mouse breeding, care, and genotyping.

**Conflicts of Interest:** The authors declare no conflict of interest.

## References

1. Desguerre, I.; Christov, C.; Mayer, M.; Zeller, R.; Becane, H.-M.; Bastuji-Garin, S.; Leturcq, F.; Chiron, C.; Chelly, J.; Gherardi, R.K. Clinical Heterogeneity of Duchenne Muscular Dystrophy (DMD): Definition of Sub-Phenotypes and Predictive Criteria by Long-Term Follow-Up. *PLoS ONE* **2009**, *4*, e4347. [[CrossRef](#)] [[PubMed](#)]
2. Perronnet, C.; Vaillend, C. Dystrophins, Utrophins, and Associated Scaffolding Complexes: Role in Mammalian Brain and Implications for Therapeutic Strategies. *J. Biomed. Biotechnol.* **2010**, *2010*, 849426. [[CrossRef](#)] [[PubMed](#)]
3. Ricotti, V.; Mandy, W.P.L.; Scoto, M.; Pane, M.; Deconinck, N.; Messina, S.; Mercuri, E.; Skuse, D.H.; Muntoni, F. Neurodevelopmental, Emotional, and Behavioural Problems in Duchenne Muscular Dystrophy in Relation to Underlying Dystrophin Gene Mutations. *Dev. Med. Child Neurol.* **2016**, *58*, 77–84. [[CrossRef](#)] [[PubMed](#)]
4. Brüning, I.; Suter, A.; Knuesel, I.; Lüscher, B.; Fritschy, J.-M. GABAergic Terminals Are Required for Postsynaptic Clustering of Dystrophin but Not of GABA(A) Receptors and Gephyrin. *J. Neurosci.* **2002**, *22*, 4805–4813. [[CrossRef](#)]
5. Fritschy, J.M.; Schweizer, C.; Brüning, I.; Lüscher, B. Pre- and Post-Synaptic Mechanisms Regulating the Clustering of Type A Gamma-Aminobutyric Acid Receptors (GABAA Receptors). *Biochem. Soc. Trans.* **2003**, *31*, 889–892. [[CrossRef](#)]
6. Knuesel, I.; Mastrocola, M.; Zuellig, R.A.; Bornhauser, B.; Schaub, M.C.; Fritschy, J.M. Short Communication: Altered Synaptic Clustering of GABAA Receptors in Mice Lacking Dystrophin (Mdx Mice). *Eur. J. Neurosci.* **1999**, *11*, 4457–4462. [[CrossRef](#)]
7. Tang, X.; Jaenisch, R.; Sur, M. The Role of GABAergic Signalling in Neurodevelopmental Disorders. *Nat. Rev. Neurosci.* **2021**, *22*, 290–307. [[CrossRef](#)]
8. Brickley, S.G.; Mody, I. Extrasynaptic GABA(A) Receptors: Their Function in the CNS and Implications for Disease. *Neuron* **2012**, *73*, 23–34. [[CrossRef](#)]
9. Duggan, M.J.; Pollard, S.; Stephenson, F.A. Immunoaffinity Purification of GABAA Receptor Alpha-Subunit Iso-Oligomers. Demonstration of Receptor Populations Containing Alpha 1 Alpha 2, Alpha 1 Alpha 3, and Alpha 2 Alpha 3 Subunit Pairs. *J. Biol. Chem.* **1991**, *266*, 24778–24784. [[CrossRef](#)]
10. Khan, Z.U.; Gutiérrez, A.; de Blas, A.L. The Alpha 1 and Alpha 6 Subunits Can Coexist in the Same Cerebellar GABAA Receptor Maintaining Their Individual Benzodiazepine-Binding Specificities. *J. Neurochem.* **1996**, *66*, 685–691. [[CrossRef](#)]

11. Benke, D.; Fakitsas, P.; Roggenmoser, C.; Michel, C.; Rudolph, U.; Mohler, H. Analysis of the Presence and Abundance of GABAA Receptors Containing Two Different Types of Alpha Subunits in Murine Brain Using Point-Mutated Alpha Subunits. *J. Biol. Chem.* **2004**, *279*, 43654–43660. [[CrossRef](#)] [[PubMed](#)]
12. Nutt, D. GABAA Receptors: Subtypes, Regional Distribution, and Function. *J. Clin. Sleep Med.* **2006**, *2*, S7–S11. [[CrossRef](#)] [[PubMed](#)]
13. Jacob, T.C.; Moss, S.J.; Jurd, R. GABA(A) Receptor Trafficking and Its Role in the Dynamic Modulation of Neuronal Inhibition. *Nat. Rev. Neurosci.* **2008**, *9*, 331–343. [[CrossRef](#)] [[PubMed](#)]
14. Pirker, S.; Schwarzer, C.; Wieselthaler, A.; Sieghart, W.; Sperk, G. GABA(A) Receptors: Immunocytochemical Distribution of 13 Subunits in the Adult Rat Brain. *Neuroscience* **2000**, *101*, 815–850. [[CrossRef](#)]
15. Laurie, D.J.; Wisden, W.; Seeburg, P.H. The Distribution of Thirteen GABAA Receptor Subunit MRNAs in the Rat Brain. III. Embryonic and Postnatal Development. *J. Neurosci.* **1992**, *12*, 4151–4172. [[CrossRef](#)] [[PubMed](#)]
16. Schneider Gasser, E.M.; Duveau, V.; Prenosil, G.A.; Fritschy, J.M. Reorganization of GABAergic Circuits Maintains GABAA Receptor-Mediated Transmission onto CA1 Interneurons in A1-Subunit-Null Mice. *Eur. J. Neurosci.* **2007**, *25*, 3287–3304. [[CrossRef](#)]
17. Fritschy, J.-M. Epilepsy, E/I Balance and GABA(A) Receptor Plasticity. *Front. Mol. Neurosci.* **2008**, *1*, 5. [[CrossRef](#)]
18. Fritschy, J.M.; Panzanelli, P.; Tyagarajan, S.K. Molecular and Functional Heterogeneity of GABAergic Synapses. *Cell. Mol. Life Sci.* **2012**, *69*, 2485–2499. [[CrossRef](#)]
19. Sekiguchi, M.; Zushida, K.; Yoshida, M.; Maekawa, M.; Kamichi, S.; Yoshida, M.; Sahara, Y.; Yuasa, S.; Takeda, S.; Wada, K. A Deficit of Brain Dystrophin Impairs Specific Amygdala GABAergic Transmission and Enhances Defensive Behaviour in Mice. *Brain* **2009**, *132*, 124–135. [[CrossRef](#)]
20. Vaillend, C.; Perronnet, C.; Ros, C.; Gruszczynski, C.; Goyenvalle, A.; Laroche, S.; Danos, O.; Garcia, L.; Peltekian, E. Rescue of a Dystrophin-like Protein by Exon Skipping in Vivo Restores GABA<sub>A</sub>-Receptor Clustering in the Hippocampus of the Mdx Mouse. *Mol. Ther.* **2010**, *18*, 1683–1688. [[CrossRef](#)]
21. Fuenzalida, M.; Espinoza, C.; Pérez, M.Á.; Tapia-Rojas, C.; Cuitino, L.; Brandan, E.; Inestrosa, N.C. Wnt Signaling Pathway Improves Central Inhibitory Synaptic Transmission in a Mouse Model of Duchenne Muscular Dystrophy. *Neurobiol. Dis.* **2016**, *86*, 109–120. [[CrossRef](#)] [[PubMed](#)]
22. Dallérac, G.; Perronnet, C.; Chagneau, C.; Leblanc-Veyrac, P.; Samson-Desvignes, N.; Peltekian, E.; Danos, O.; Garcia, L.; Laroche, S.; Billard, J.-M.; et al. Rescue of a Dystrophin-like Protein by Exon Skipping Normalizes Synaptic Plasticity in the Hippocampus of the Mdx Mouse. *Neurobiol. Dis.* **2011**, *43*, 635–641. [[CrossRef](#)] [[PubMed](#)]
23. Vaillend, C.; Chausseot, R. Relationships Linking Emotional, Motor, Cognitive and GABAergic Dysfunctions in Dystrophin-Deficient Mdx Mice. *Hum. Mol. Genet.* **2017**, *26*, 1041–1055. [[CrossRef](#)] [[PubMed](#)]
24. Kueh, S.L.L.; Head, S.I.; Morley, J.W. GABAA Receptor Expression and Inhibitory Post-Synaptic Currents in Cerebellar Purkinje Cells in Dystrophin-Deficient Mdx Mice. *Clin. Exp. Pharmacol. Physiol.* **2008**, *35*, 207–210. [[CrossRef](#)]
25. Vaillend, C.; Billard, J.M. Facilitated CA1 Hippocampal Synaptic Plasticity in Dystrophin-Deficient Mice: Role for GABAA Receptors? *Hippocampus* **2002**, *12*, 713–717. [[CrossRef](#)] [[PubMed](#)]
26. Graciotti, L.; Minelli, A.; Minciacchi, D.; Procopio, A.; Fulgenzi, G. GABAergic Miniature Spontaneous Activity Is Increased in the CA1 Hippocampal Region of Dystrophic Mdx Mice. *Neuromuscul. Disord.* **2008**, *18*, 220–226. [[CrossRef](#)]
27. de Sarro, G.; Ibbadu, G.F.; Marra, R.; Rotiroli, D.; Loiacono, A.; Donato Di Paola, E.; Russo, E. Seizure Susceptibility to Various Convulsant Stimuli in Dystrophin-Deficient Mdx Mice. *Neurosci. Res.* **2004**, *50*, 37–44. [[CrossRef](#)]
28. Wu, W.-C.; Bradley, S.P.; Christie, J.M.; Pugh, J.R. Mechanisms and Consequences of Cerebellar Purkinje Cell Disinhibition in a Mouse Model of Duchenne Muscular Dystrophy. *J. Neurosci.* **2022**, *42*, 2103–2115. [[CrossRef](#)]
29. Kueh, S.L.L.; Dempster, J.; Head, S.I.; Morley, J.W. Reduced Postsynaptic GABAA Receptor Number and Enhanced Gaboxadol Induced Change in Holding Currents in Purkinje Cells of the Dystrophin-Deficient Mdx Mouse. *Neurobiol. Dis.* **2011**, *43*, 558–564. [[CrossRef](#)]
30. Zarrouki, F.; Relizani, K.; Bizot, F.; Tensorer, T.; Garcia, L.; Vaillend, C.; Goyenvalle, A. Partial Restoration of Brain Dystrophin and Behavioral Deficits by Exon Skipping in the Muscular Dystrophy X-Linked (Mdx) Mouse. *Ann. Neurol.* **2022**, *92*, 213–229. [[CrossRef](#)]
31. Goyenvalle, A.; Griffith, G.; Babbs, A.; El Andaloussi, S.; Ezzat, K.; Avril, A.; Dugovic, B.; Chausseot, R.; Ferry, A.; Voit, T.; et al. Functional Correction in Mouse Models of Muscular Dystrophy Using Exon-Skipping Tricyclo-DNA Oligomers. *Nat. Med.* **2015**, *21*, 270–275. [[CrossRef](#)] [[PubMed](#)]
32. Juhász, C.; Chugani, D.C.; Muzik, O.; Shah, A.; Shah, J.; Watson, C.; Canady, A.; Chugani, H.T. Relationship of Flumazenil and Glucose PET Abnormalities to Neocortical Epilepsy Surgery Outcome. *Neurology* **2001**, *56*, 1650–1658. [[CrossRef](#)] [[PubMed](#)]
33. Hammers, A.; Panagoda, P.; Heckemann, R.A.; Kelsch, W.; Turkheimer, F.E.; Brooks, D.J.; Duncan, J.S.; Koeppe, M.J. [<sup>11</sup>C]Flumazenil PET in Temporal Lobe Epilepsy: Do We Need an Arterial Input Function or Kinetic Modeling? *J. Cereb. Blood Flow Metab.* **2008**, *28*, 207–216. [[CrossRef](#)] [[PubMed](#)]
34. Müller Herde, A.; Benke, D.; Ralvenius, W.T.; Mu, L.; Schibli, R.; Zeilhofer, H.U.; Krämer, S.D. GABA A Receptor Subtypes in the Mouse Brain: Regional Mapping and Diazepam Receptor Occupancy by in Vivo [<sup>18</sup>F]Flumazenil PET. *Neuroimage* **2017**, *150*, 279–291. [[CrossRef](#)]

35. Froklage, F.E.; Postnov, A.; Yaqub, M.M.; Bakker, E.; Boellaard, R.; Harry Hendrikse, N.; Comans, E.F.I.; Schuit, R.C.; Schober, P.; Velis, D.N.; et al. Altered GABAA Receptor Density and Unaltered Blood-Brain Barrier [11C]Flumazenil Transport in Drug-Resistant Epilepsy Patients with Mesial Temporal Sclerosis. *J. Cereb. Blood Flow Metab.* **2017**, *37*, 97–105. [[CrossRef](#)]
36. Asiedu, M.N.; Mejia, G.; Ossipov, M.K.; Malan, T.P.; Kaila, K.; Price, T.J. Modulation of Spinal GABAergic Analgesia by Inhibition of Chloride Extrusion Capacity in Mice. *J. Pain* **2012**, *13*, 546–554. [[CrossRef](#)] [[PubMed](#)]
37. Munro, G.; Lopez-Garcia, J.A.; Rivera-Arconada, I.; Erichsen, H.K.; Nielsen, E.; Larsen, J.S.; Ahring, P.K.; Mirza, N.R. Comparison of the Novel Subtype-Selective GABAA Receptor-Positive Allosteric Modulator NS11394 [3'-(5-(1-Hydroxy-1-Methyl-Ethyl)-Benzoimidazol-1-Yl)-Biphenyl-2-Carbonitrile] with Diazepam, Zolpidem, Bretazenil, and Gaboxadol in Rat Models of Inflammatory and Neuropathic Pain. *J. Pharmacol. Exp. Ther.* **2008**, *327*, 969–981. [[CrossRef](#)] [[PubMed](#)]
38. Lidov, H.G.; Byers, T.J.; Kunkel, L.M. The Distribution of Dystrophin in the Murine Central Nervous System: An Immunocytochemical Study. *Neuroscience* **1993**, *54*, 167–187. [[CrossRef](#)]
39. Krasowska, E.; Zabłocki, K.; Górecki, D.C.; Swinny, J.D. Aberrant Location of Inhibitory Synaptic Marker Proteins in the Hippocampus of Dystrophin-Deficient Mice: Implications for Cognitive Impairment in Duchenne Muscular Dystrophy. *PLoS ONE* **2014**, *9*, e108364. [[CrossRef](#)]
40. Suzuki, Y.; Higuchi, S.; Aida, I.; Nakajima, T.; Nakada, T. Abnormal Distribution of GABAA Receptors in Brain of Duchenne Muscular Dystrophy Patients. *Muscle Nerve* **2017**, *55*, 591–595. [[CrossRef](#)]
41. Hendriksen, R.G.F.; Hoogland, G.; Schipper, S.; Hendriksen, J.G.M.; Vles, J.S.H.; Aalbers, M.W. A Possible Role of Dystrophin in Neuronal Excitability: A Review of the Current Literature. *Neurosci. Biobehav. Rev.* **2015**, *51*, 255–262. [[CrossRef](#)] [[PubMed](#)]
42. De Stefano, M.E.; Ferretti, V.; Mozzetta, C. Synaptic Alterations as a Neurodevelopmental Trait of Duchenne Muscular Dystrophy. *Neurobiol. Dis.* **2022**, *168*, 105718. [[CrossRef](#)] [[PubMed](#)]
43. Lu, F.-M.; Yuan, Z. PET/SPECT Molecular Imaging in Clinical Neuroscience: Recent Advances in the Investigation of CNS Diseases. *Quant. Imaging Med. Surg.* **2015**, *5*, 433–447. [[CrossRef](#)] [[PubMed](#)]
44. Kneussel, M.; Loeblich, S. Trafficking and Synaptic Anchoring of Ionotropic Inhibitory Neurotransmitter Receptors. *Biol. Cell* **2007**, *99*, 297–309. [[CrossRef](#)] [[PubMed](#)]
45. Marques, T.R.; Ashok, A.H.; Angelescu, I.; Borgan, F.; Myers, J.; Lingford-Hughes, A.; Nutt, D.J.; Veronese, M.; Turkheimer, F.E.; Howes, O.D. GABA-A Receptor Differences in Schizophrenia: A Positron Emission Tomography Study Using [11 C]Ro154513. *Mol. Psychiatry* **2021**, *26*, 2616–2625. [[CrossRef](#)]
46. Olsen, R.W.; Sieghart, W. GABA A Receptors: Subtypes Provide Diversity of Function and Pharmacology. *Neuropharmacology* **2009**, *56*, 141–148. [[CrossRef](#)]
47. Lévi, S.; Grady, R.M.; Henry, M.D.; Campbell, K.P.; Sanes, J.R.; Craig, A.M. Dystroglycan Is Selectively Associated with Inhibitory GABAergic Synapses but Is Dispensable for Their Differentiation. *J. Neurosci.* **2002**, *22*, 4274–4285. [[CrossRef](#)]
48. Panzanelli, P.; Früh, S.; Fritschy, J.M. Differential Role of GABA A Receptors and Neuroligin 2 for Perisomatic GABAergic Synapse Formation in the Hippocampus. *Brain Struct. Funct.* **2017**, *222*, 4149–4161. [[CrossRef](#)]
49. Sumita, K.; Sato, Y.; Iida, J.; Kawata, A.; Hamano, M.; Hirabayashi, S.; Ohno, K.; Peles, E.; Hata, Y. Synaptic Scaffolding Molecule (S-SCAM) Membrane-Associated Guanylate Kinase with Inverted Organization (MAGI)-2 Is Associated with Cell Adhesion Molecules at Inhibitory Synapses in Rat Hippocampal Neurons. *J. Neurochem.* **2007**, *100*, 154–166. [[CrossRef](#)]
50. Wallis, T.; Bubb, W.A.; McQuillan, J.A.; Balcar, V.J.; Rae, C. For Want of a Nail. Ramifications of a Single Gene Deletion, Dystrophin, in the Brain of the Mouse. *Front. Biosci.* **2004**, *9*, 74–84. [[CrossRef](#)]
51. Assis, A.D.; Chiarotto, G.B.; Simões, G.F.; Oliveira, A.L.R. Pregabalin-Induced Neuroprotection and Gait Improvement in Dystrophic MDX Mice. *Mol. Cell Neurosci.* **2021**, *114*, 103632. [[CrossRef](#)] [[PubMed](#)]
52. Meera, P.; Wallner, M.; Otis, T.S. Molecular Basis for the High THIP/Gaboxadol Sensitivity of Extrasynaptic GABA(A) Receptors. *J. Neurophysiol.* **2011**, *106*, 2057–2064. [[CrossRef](#)] [[PubMed](#)]
53. Saarelainen, K.S.; Ranna, M.; Rabe, H.; Sinkkonen, S.T.; Möykkynen, T.; Uusi-Oukari, M.; Linden, A.-M.; Lüddens, H.; Korpi, E.R. Enhanced Behavioral Sensitivity to the Competitive GABA Agonist, Gaboxadol, in Transgenic Mice over-Expressing Hippocampal Extrasynaptic Alpha6beta GABA(A) Receptors. *J. Neurochem.* **2008**, *105*, 338–350. [[CrossRef](#)]
54. Delgado-Lezama, R.; Loeza-Alcocer, E.; Andres, C.; Aguilar, J.; Guertin, P.; Felix, R. Extrasynaptic GABA(A) Receptors in the Brainstem and Spinal Cord: Structure and Function. *Curr. Pharm. Des.* **2013**, *19*, 4485–4497. [[CrossRef](#)] [[PubMed](#)]
55. Hausrat, T.J.; Muhia, M.; Gerrow, K.; Thomas, P.; Hirdes, W.; Tsukita, S.; Heisler, F.F.; Herich, L.; Dubroqua, S.; Breiden, P.; et al. Radixin Regulates Synaptic GABAA Receptor Density and Is Essential for Reversal Learning and Short-Term Memory. *Nat. Commun.* **2015**, *6*, 6872. [[CrossRef](#)]
56. Damgaard, T.; Plath, N.; Neill, J.C.; Hansen, S.L. Extrasynaptic GABAA Receptor Activation Reverses Recognition Memory Deficits in an Animal Model of Schizophrenia. *Psychopharmacology* **2011**, *214*, 403–413. [[CrossRef](#)]
57. Shen, H.; Sabaliauskas, N.; Yang, L.; Aoki, C.; Smith, S.S. Role of A4-Containing GABA A Receptors in Limiting Synaptic Plasticity and Spatial Learning of Female Mice during the Pubertal Period. *Brain Res.* **2017**, *1654*, 116–122. [[CrossRef](#)]
58. Moore, M.D.; Cushman, J.; Chandra, D.; Homanics, G.E.; Olsen, R.W.; Fanselow, M.S. Trace and Contextual Fear Conditioning Is Enhanced in Mice Lacking the Alpha4 Subunit of the GABA(A) Receptor. *Neurobiol. Learn Mem.* **2010**, *93*, 383–387. [[CrossRef](#)]
59. Chen, X.; van Gerven, J.; Cohen, A.; Jacobs, G. Human Pharmacology of Positive GABA-A Subtype-Selective Receptor Modulators for the Treatment of Anxiety. *Acta Pharmacol. Sin.* **2019**, *40*, 571–582. [[CrossRef](#)]

60. Sieghart, W.; Chiou, L.C.; Ernst, M.; Fabjan, J.; Savić, M.M.; Lee, M.T.  $\alpha$  6-Containing GABA A Receptors: Functional Roles and Therapeutic Potentials. *Pharmacol. Rev.* **2022**, *74*, 238–270. [[CrossRef](#)]
61. Evrard, M.R.; Li, M.; Shen, H.; Smith, S.S. Preventing Adolescent Synaptic Pruning in Mouse Prelimbic Cortex via Local Knockdown of A4 $\beta$  $\delta$  GABA A Receptors Increases Anxiety Response in Adulthood. *Sci. Rep.* **2021**, *11*, 21059. [[CrossRef](#)] [[PubMed](#)]
62. Bannai, H.; Lévi, S.; Schweizer, C.; Inoue, T.; Launey, T.; Racine, V.; Sibarita, J.B.; Mikoshiba, K.; Triller, A. Activity-Dependent Tuning of Inhibitory Neurotransmission Based on GABAAR Diffusion Dynamics. *Neuron* **2009**, *62*, 670–682. [[CrossRef](#)] [[PubMed](#)]
63. Alcor, D.; Gouzer, G.; Triller, A. Single-Particle Tracking Methods for the Study of Membrane Receptors Dynamics. *Eur. J. Neurosci.* **2009**, *30*, 987–997. [[CrossRef](#)] [[PubMed](#)]
64. Bouzigues, C.; Morel, M.; Triller, A.; Dahan, M. Asymmetric Redistribution of GABA Receptors during GABA Gradient Sensing by Nerve Growth Cones Analyzed by Single Quantum Dot Imaging. *Proc. Natl. Acad. Sci. USA* **2007**, *104*, 11251–11256. [[CrossRef](#)]
65. Lorenz-Guertin, J.M.; Jacob, T.C. GABA Type a Receptor Trafficking and the Architecture of Synaptic Inhibition. *Dev. Neurobiol.* **2018**, *78*, 238–270. [[CrossRef](#)]
66. Ma, Y.; Hof, P.R.; Grant, S.C.; Blackband, S.J.; Bennett, R.; Slatest, L.; Mcguigan, M.D.; Benveniste, H. A Three-Dimensional Digital Atlas Database of the Adult C57BL/6j Mouse Brain by Magnetic Resonance Microscopy. *Neuroscience* **2005**, *135*, 1203–1215. [[CrossRef](#)]
67. Paxinos, G.F.K. *The Mouse Brain in Stereotaxic Coordinates*, 2nd ed.; Academic Press: San Diego, CA, USA, 2001.
68. Früh, S.; Romanos, J.; Panzanelli, P.; Bürgisser, D.; Tyagarajan, S.K.; Campbell, K.P.; Santello, M.; Fritschy, J.M. Neuronal Dystroglycan Is Necessary for Formation and Maintenance of Functional CCK-Positive Basket Cell Terminals on Pyramidal Cells. *J. Neurosci.* **2016**, *36*, 10296–10313. [[CrossRef](#)]
69. Sassoè-Pognetto, M.; Panzanelli, P.; Sieghart, W.; Fritschy, J.M. Colocalization of Multiple GABA(A) Receptor Subtypes with Gephyrin at Postsynaptic Sites. *J. Comp. Neurol.* **2000**, *420*, 481–498. [[CrossRef](#)]
70. Beekman, C.; Janson, A.A.; Baghat, A.; van Deutekom, J.C.; Datson, N.A. Use of Capillary Western Immunoassay (Wes) for Quantification of Dystrophin Levels in Skeletal Muscle of Healthy Controls and Individuals with Becker and Duchenne Muscular Dystrophy. *PLoS ONE* **2018**, *13*, e0195850. [[CrossRef](#)]